Title

Click chemistry-mediated enrichment of circulating tumor cells and tumor-derived extracellular vesicles for dual liquid biopsy in differentiated thyroid cancer

Authors

Feng, Bing
Wang, Jing
Zhang, Ryan Y
et al.

Publication Date

2024-10-01

DOI

10.1016/j.nantod.2024.102431

Click Chemistry-Mediated Enrichment of Circulating Tumor Cells and Tumor-Derived Extracellular Vesicles for Dual Liquid Biopsy in Differentiated Thyroid Cancer

Bing Feng [a,b,c], Jing Wang [c], Ryan Y. Zhang [c], Anna Yaxuan Wei [c], Chen Zhao [a,c], Ying-Tzu Yen [a,c], You-Ren Ji [c], Hyoyong Kim [c], Yong Ju [c], Matthew Smalley [c], Vivian Xufei Zuo [c], Liwen Cheng [c], Aaron Phung [c], Ziang Zhou [c], Sitong Yu [c], Gabriella DiBernardo [d,e,l], Sanaz Memarzadeh [d,e,f,g,l], Edwin M. Posadas [h], Wanxing Chai-Ho [i], Vatche Agopian [j], Junseok Lee [c], Michael W. Yeh [j,l], James Wu [j,l,*], Guangjuan Zheng [b,k,**], Hsian-Rong Tseng [c,l,***], Yazhen Zhu [a,c,l,****]

[a] *Department of Pathology and Laboratory Medicine, David Geffen School of Medicine, University of California, Los Angeles, 570 Westwood Plaza, Los Angeles, California 90095, USA*

[b] *State Key Laboratory of Dampness Syndrome of Chinese Medicine, Guangdong-Hong Kong-Macau Joint Lab on Chinese Medicine and Immune Disease Research, Guangdong Provincial Hospital of Chinese Medicine, The Second Affiliated Hospital of Guangzhou University of Chinese Medicine, Guangzhou University of Chinese Medicine, 111 Dade Road, Guangzhou, Guangdong 510120, China*

[c] *California NanoSystems Institute, Crump Institute for Molecular Imaging, Department of Molecular and Medical Pharmacology, University of California, Los Angeles, 570 Westwood Plaza, Los Angeles, California 90095, USA*

[d] *Department of Obstetrics and Gynecology, David Geffen School of Medicine, University of California, Los Angeles, 200 Medical Plaza, Los Angeles, California 90024, USA*

[e] *Eli and Edythe Broad Center of Regenerative Medicine and Stem Cell Research, University of California, Los Angeles, 617 Charles E. Young Drive East, Los Angeles, California 90095, USA*

[f] *Molecular Biology Institute, University of California, Los Angeles, 611 Charles E. Young Drive East, Los Angeles, California 90095, USA*

[g] *The VA Greater Los Angeles Healthcare System, 11301 Wilshire Blvd., Los Angeles, California 90073, USA*

[h] *Division of Medical Oncology, Department of Medicine, Cedars-Sinai Medical Center, 127 S San Vicente Blvd, Los Angeles, California 90048, USA*

[i] *Department of Medicine, Division of Hematology/Oncology, David Geffen School of Medicine, University of California, Los Angeles, 200 Medical Plaza, Los Angeles, California 90024, USA*

[j] *Department of Surgery, David Geffen School of Medicine, University of California, Los Angeles, 200 Medical Plaza, Los Angeles, California 90024, USA*

[k] *Department of Pathology, Guangdong Provincial Hospital of Chinese Medicine, 111 Dade Road, Guangzhou, Guangdong 510120, China*

[l] *Jonsson Comprehensive Cancer Center, University of California, Los Angeles, California 90095, USA*

* Corresponding author at: Department of Surgery, David Geffen School of Medicine, University of California, Los Angeles, 200 Medical Plaza, Los Angeles, California 90024, USA.

** Corresponding author at: State Key Laboratory of Dampness Syndrome of Chinese Medicine, Guangdong-Hong Kong-Macau Joint Lab on Chinese Medicine and Immune Disease Research, Guangdong Provincial Hospital of Chinese Medicine, The Second Affiliated Hospital of Guangzhou University of Chinese Medicine, Guangzhou University of Chinese Medicine, 111 Dade Road, Guangzhou, Guangdong 510120, China.

*** Corresponding author at: California NanoSystems Institute, Crump Institute for Molecular Imaging, Department of Molecular and Medical Pharmacology, University of California, Los Angeles, 570 Westwood Plaza, Los Angeles, California 90095, USA.

**** Corresponding author at: Department of Pathology and Laboratory Medicine, David Geffen School of Medicine, University of California, Los Angeles, 570 Westwood Plaza, Los Angeles, California 90095, USA.

E-mail addresses: jameswu@mednet.ucla.edu (J. Wu), zhengguangjuan@gzucm.edu.cn (G. Zheng), hrtseng@mednet.ucla.edu (H.-R. Tseng), yazhenzhu@mednet.ucla.edu (Y. Zhu).

Highlights

1. Click chemistry-mediated enrichment platforms can efficiently enrich DTC CTCs/^{t}EVs
2. A DTC CTC-derived mRNA signature can be quantified by RT-dPCR
3. Three DTC ^{t}EV subpopulations can be indirectly quantified by RT-qPCR
4. The Combined DTC CTC/^{t}EV Assay shows remarkable diagnostic accuracy for detecting DTC

Abstract:

Circulating tumor cells (CTCs) and tumor-derived extracellular vesicles (^{t}EVs) are two crucial methodologies of liquid biopsy. Given their distinct size differences and release dynamics, CTCs and ^{t}EVs potentially offer synergistic capabilities in the non-invasive detection of differentiated thyroid cancer (DTC), a typically indolent tumor. We present the Combined DTC CTC/^{t}EV Assay, integrating dual liquid biopsy processes: i) DTC CTC enrichment by Click Chips, followed by analysis of seven DTC-specific genes, and ii) DTC ^{t}EV enrichment by Click Beads, succeeded by mRNA cargo quantification in DTC ^{t}EVs. This method utilizes click chemistry, leveraging a pair of biorthogonal and highly reactive functional motifs (tetrazine, Tz, and trans-cyclooctene, TCO), to overcome the challenges encountered in the conventional immunoaffinity-based enrichment of CTCs and ^{t}EVs. The Combined DTC CTC/^{t}EV Assay synergistically combines the diagnostic precision of CTCs with the sensitivity of ^{t}EVs, demonstrating superior diagnostic accuracy in DTC detection and boasting an AUROC of 0.99. This outperforms the individual diagnostic performance of using either DTC CTC or DTC ^{t}EV alone. This integration enables full utilization of a patient's blood sample, and marks a significant evolution in the development of nanomaterial-based liquid biopsy technologies to address challenging unmet clinical needs in cancer care.

Keywords:

Click chemistry

Circulating tumor cells

Extracellular vesicles

Liquid biopsy

Differentiated thyroid cancer

1. Introduction

In the field of oncology, liquid biopsy typically examines various components in the blood or other body fluids [1-6], including circulating tumor cells (CTCs) [7, 8], tumor-derived extracellular vesicles (ᵗEVs) [9-12], or nucleic acid released from tumors, such as cell-free DNA , microRNA [13], and non-coding RNA [14]. Compared to cell-free DNA and RNA, CTCs and ᵗEVs possess lipid bilayer membranes, which both harbor surface markers that mirror those on tumor cell surfaces [15], and protect fragile biomolecular cargos (e.g., mRNA) from degradation [16, 17]. Considering the intrinsic size differences between CTCs and ᵗEVs (which determine their underlying releasing mechanisms as well as the timing of their release into the circulation), CTCs and ᵗEVs could offer complementary roles for cancer diagnostic applications [18-20]. Synergically integrating the mRNA signatures derived from CTCs and ᵗEVs could enhance the sensitivity and specificity of this integrated diagnostic approach and allow full utilization of a single patient's blood sample. Thus, there is a crucial need to develop novel technologies to enrich CTCs and ᵗEVs [21, 22], in parallel with a high degree of sensitivity/specificity while preserving mRNA integrity.

Significant research efforts have been devoted to exploring immunoaffinity-based capture techniques targeting surface markers for the specific enrichment of CTCs [23-27] and ᵗEVs [22, 28-30]. However, there remain technical challenges with immunoaffinity-mediated enrichment of CTCs and/or ᵗEVs, such as limited sensitivity/specificity and the need for multiple enrichment antibodies to address tumor heterogeneity. To overcome these challenges, our research team has developed technologies utilizing click chemistry for the enrichment of both CTCs through Click Chips [31] and ᵗEVs through Click Beads [32]. Here, click chemistry is based on a pair of biorthogonal and highly reactive functional motifs (i.e., tetrazine, Tz, and trans-cyclooctene, TCO) [33, 34] that are grafted onto CTC/ᵗEV-enrichment substrates (via surface modification) and CTCs/ᵗEVs (via conjugation antibodies targeting designated tumor surface markers), respectively. When TCO-grafted CTCs/ᵗEVs approach to the enrichment substrates, the inverse-electron-demand Diels-Alder reaction (between TCO on CTCs/ᵗEVs and Tz on the substrates) [35, 36] leads to irreversible immobilization of CTCs/ᵗEVs with dramatically improved sensitivity and specificity. The enriched CTCs and ᵗEVs can be subjected to subsequent mRNA profiling and bioinformatics analysis, enabling early diagnosis [32], treatment monitoring [31], and assessment of prognosis for various types of tumors [30, 37, 38]. The combined use of these two click chemistry-mediated CTCs/ᵗEVs

enrichment platforms will facilitate the exploration of the synergistic roles of CTCs and tEVs to achieve further improved diagnostic performance crucial for detecting challenging early-stage indolent tumors that may otherwise remain undetectable with a single platform alone.

The incidence of thyroid cancer has risen sharply, with a 300% increase in incidence in the past three decades [39, 40]. Differentiated thyroid cancers (DTCs), account for 90% of all thyroid cancer cases, are epithelial tumors that typically arise from thyroid follicular cells, including papillary thyroid carcinoma (PTC) and follicular thyroid carcinoma (FTC) [41]. Liquid biopsy can enhance diagnostic and prognostic strategies for DTC in a noninvasive manner [42]. However, DTCs are well differentiated histologically with relatively indolent tumor growth [43], posing a significant challenge for their detection through liquid biopsy [44]. Therefore, it is crucial to develop highly sensitive assays for detecting thyroid cancer in liquid biopsy settings. In light of the complementary roles of CTCs and tEVs in DTC, we developed a Combined DTC CTC/tEV Assay, which synergistically integrated click chemistry-mediated enrichment of DTC CTCs and tEVs from any given blood sample, enabling subsequent molecular characterization and quantification.

In this study, we developed the Combined DTC CTC/tEV Assay by integrating dual liquid biopsy processes, including i) click chemistry-mediated DTC CTC enrichment from patients' peripheral blood mononuclear cell (PBMC) samples, followed by quantification of the seven DTC-specific genes, and ii) click chemistry-mediated DTC tEV enrichment from the same patients' plasma samples, followed by quantification of mRNA cargo within DTC tEVs (**Fig. 1**). Firstly, in the presence of two TCO-grafted DTC-associated antibodies (i.e., TCO-anti-CD147 and TCO-anti-EpCAM), click chemistry-mediated enrichment was adopted to immobilize DTC CTCs onto Tz-grafted Click Chips using DTC patients' PBMC samples. Subsequently, these enriched DTC CTCs were lysed to extract mRNA. The resultant DTC CTC-derived mRNA was then subjected to analysis by reverse transcription digital polymerase chain reaction (RT-dPCR) to quantify a panel of seven DTC-specific genes, including *TG*, *TPO*, *SLC26A4*, *IYD*, *SLC26A7*, *TSHR*, and *FOXE1*. These seven genes were identified via a bioinformatic workflow based on human thyroid gland transcriptome datasets from the Human Protein Atlas (**Fig. 2B**) and have now been validated as DTC-specific genes when present in peripheral blood samples. Second, in conjunction with the use of one of the four TCO-grafted DTC-associated antibodies (i.e., TCO-anti-CD147, TCO-anti-EpCAM, TCO-anti-B7H3, or TCO-anti-MUC1), click chemistry-mediated enrichment was employed

to immobilize a respective subpopulation of DTC ᵗEVs onto Tz-grafted Click Beads using DTC patients' plasma samples. Next, the enriched DTC ᵗEVs were lysed to release DTC ᵗEV-derived mRNA. Reverse transcription quantitative polymerase chain reaction (RT-qPCR) was used to quantify β-actin mRNA in the DTC ᵗEVs, allowing for quantification of subpopulations of DTC ᵗEVs (i.e., $CD147^+$ DTC ᵗEVs, $EpCAM^+$ DTC ᵗEVs, $B7H3^+$ DTC ᵗEVs, and $MUC1^+$ DTC ᵗEVs). Finally, 38 DTC patients and 21 healthy donors (HDs) were recruited to examine the diagnostic capacity of the Combined DTC CTC/ᵗEV Assay. Each blood sample was first separated into a PBMC sample and a plasma sample. Subsequently, DTC CTCs were enriched from PBMCs using Click Chips, while DTC ᵗEVs were enriched from plasma using Click Beads. These DTC CTCs and DTC ᵗEVs were then subjected to the Combined DTC CTC/ᵗEV Assay to generate DTC CTC-derived gene signatures and provide quantitative readouts of subpopulations of DTC ᵗEVs. Biostatistical analysis was performed to calculate Combined DTC CTC/ᵗEV Scores, and the results demonstrated that the Combined DTC CTC/ᵗEV Assay can be effectively used for distinguishing DTC patients from HDs, achieving an impressive area under Receiver Operating Characteristic Curve (AUROC) of 0.99, along with high sensitivity (95%) and specificity (95%). This approach holds great promise to significantly enhance the capabilities of current DTC diagnostic modalities.

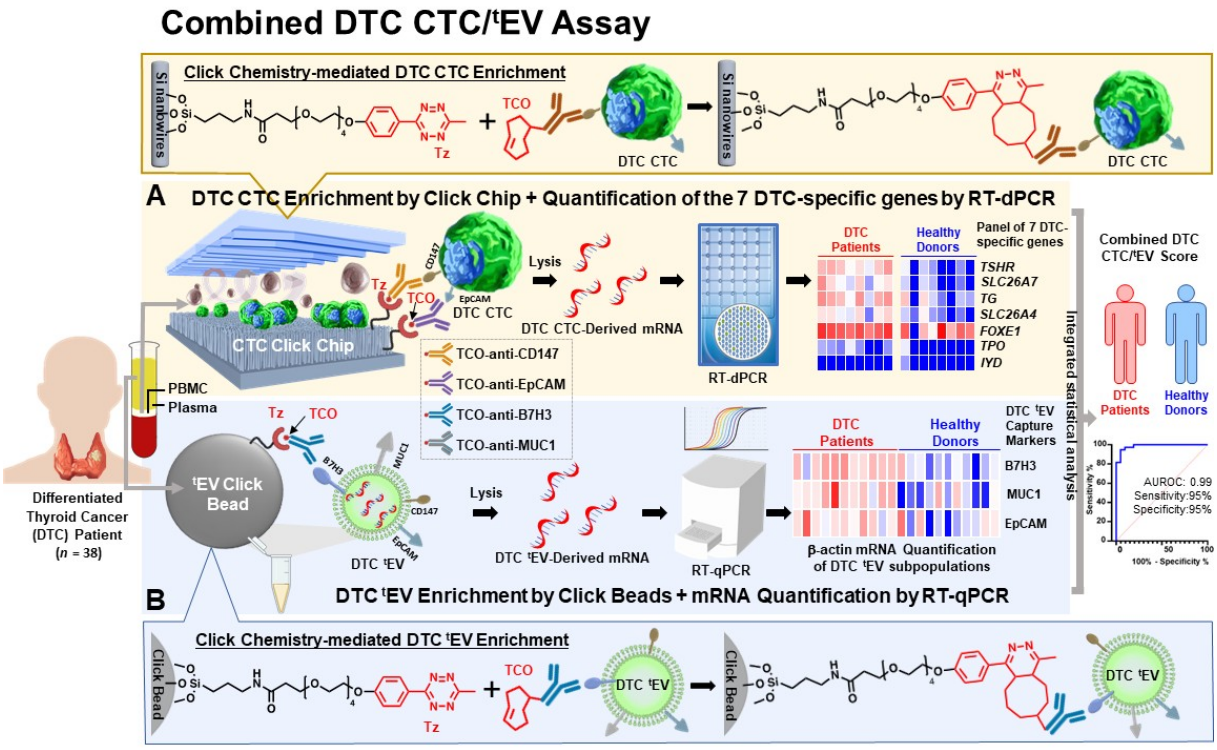

Fig. 1. Schematic illustration of the Combined DTC CTC/ᵗEV Assay for detecting patients with differentiated thyroid cancer (DTC). A) DTC CTC Enrichment by Click Chip + Quantification of the Seven DTC-specific genes by RT-dPCR. In the presence of two TCO-grafted DTC-associated antibodies (i.e., TCO-anti-CD147 and TCO-anti-EpCAM), click chemistry-mediated CTC enrichment was adopted to enrich DTC CTCs from DTC patients' PBMCs. The DTC CTCs were then lysed to extract DTC CTC-derived mRNA, followed by RT-dPCR for quantification of seven DTC-specific genes in DTC patients and healthy donors (HDs). **B) DTC ᵗEV Enrichment by Click Beads + mRNA Quantification by RT-qPCR.** In conjunction with the use of one of the four TCO-grafted DTC-associated antibodies (i.e., TCO-anti-CD147, TCO-anti-EpCAM, TCO-anti-B7H3, or TCO-anti-MUC1), click chemistry-mediated ᵗEV enrichment was adopted to enrich subpopulations of DTC ᵗEVs using Click Beads. The enriched DTC ᵗEVs were then lysed to release DTC ᵗEV-derived mRNA for quantification of β-actin by RT-qPCR. Finally, an integrated statistical analysis was performed to generate Combined DTC CTC/ᵗEV Scores for DTC detection.

2. Results and Discussions

2.1 Selection and Validation of DTC-Associated Surface Markers for Enrichment of DTC CTCs and DTC ᵗEVs

A key step towards achieving successful enrichment of DTC CTCs from PBMCs with Click Chips and DTC ᵗEVs from plasma with Click Beads is to identify a small collection of DTC-associated surface markers to specifically target and enrich DTC CTCs and DTC ᵗEVs [45, 46]. Numerous studies have previously established the effectiveness of targeting EpCAM, a

widely-used surface marker, for enriching CTCs in various epithelial-origin solid tumors [47-51]. Similarly, CD147 has also been adopted for targeting and enriching CTCs of epithelial origin [31, 52, 53]. Moreover, both EpCAM and CD147 exhibit differentially high expression in DTC tissues compared to normal tissues [54, 55]. We therefore combined anti-EpCAM and anti-CD147 in a cocktail to pair with Click Chips for DTC CTC enrichment. To further confirm that there is sufficient expression of EpCAM and CD147 on the DTC cell surfaces, we carried out immunofluorescence staining of anti-EpCAM and anti-CD147 on three thyroid cancer cell lines, i.e., MDA-T32, KTC1, and BCPAP. The fluorescent micrographs (**Fig. S1A**) revealed specific expression of EpCAM and CD147 on the surfaces of all three thyroid cancer cell lines, contrasting with their absence on the PBMCs from HDs.

Given that both DTC CTCs and DTC ᵗEVs share surface markers with their parental DTC tumor, we used anti-EpCAM and anti-CD147, previously identified for DTC CTC enrichment, to enrich DTC ᵗEVs. However, given the significantly smaller surface areas of ᵗEVs in comparison to CTCs, it is evident that ᵗEVs have fewer surface markers on their surface membranes. This could result in a lower availability of surface markers for click chemistry-mediated enrichment [56, 57]. Further, because of the heterogeneity of tumors, ᵗEVs—as their secreted products—also comprise heterogeneous subpopulations [58, 59], underscoring the importance of incorporating additional surface markers to cover the highly heterogenous subpopulations of DTC ᵗEVs. Recent studies have demonstrated that B7H3 and MUC1 have been extensively adopted as ᵗEV surface markers for enriching ᵗEVs in many solid tumors [60, 61]. Further, both B7H3 and MUC1 are highly expressed in DTC tissues compared to the normal tissues [62-64]. Hence, we explored both B7H3 and MUC1 as additional candidate surface markers for enriching DTC ᵗEVs. **Fig. S1B** illustrates that B7H3 and MUC1 were specific surface markers expressed on all three thyroid cancer cell lines (i.e., MDA-T32, KTC1, and BCPAP) but were absent on the PBMCs from HDs.

2.2 Optimization of Click Chips for the Enrichment of DTC CTCs

Click Chips were first developed for conducting click chemistry-mediated CTC enrichment, allowing for instant purification of non-small cell lung cancer (NSCLC) CTCs [31] and hepatocellular carcinoma (HCC) CTCs [46] with well-preserved mRNA that allowed for downstream target gene quantification by RT-ddPCR and NanoString, respectively. Click

Chips feature a device configuration with two functional components housed in a chip holder **(Fig. 1A):** a Tz-grafted silicon nanowire substrates (SiNWS) and an overlaid polydimethylsiloxane (PDMS)-based chaotic mixer. The embedded silicon nanowires (100–200 nm in diameter and 5-10 μm in length) were introduced onto a silicon wafer through photolithographic patterning, followed by silver (Ag) nanoparticle-templated etching [65]. After modification by Tz motif, the densely packed silicon nanowires provide a large surface area for click chemistry-mediated DTC CTC enrichment.

Efficient enrichment of DTC CTCs by Click Chips depends on using optimal concentrations of TCO-grafted DTC-associated antibodies. To optimize the enrichment efficiency of Tz-grafted Click Chips and TCO-grafted DTC-associated antibodies, we generated artificial DTC PBMC samples (**Fig. S2A**) by spiking 200 MDA-T32 cells (labeled with Vybrant DiD, a cell membrane dye, red color) into PBMCs isolated from a HD's blood. Subsequently, these artificial DTC PBMC samples (in 200 μL PBS) were incubated with a single antibody or the antibody cocktail using TCO-grafted DTC-associated antibodies (i.e., TCO-anti-EpCAM or/and TCO-anti-CD147) and then introduced into Click Chips at a flow rate [66] of 0.5 mL h^{-1} to enrich for DTC CTCs. Following staining with 4',6-diamidino-2-phenylindole (DAPI), both the DiD-labeled MDA-T32 cells and the background PBMCs were scanned and imaged using a fluorescent microscope (Nikon 90i). The efficiencies of DTC CTC enrichment were determined by dividing the number of DTC CTCs enriched on Click Chips by the number of target cells initially introduced into the artificial PBMC samples. We first assessed the impact of varying the amount of TCO-anti-EpCAM (i.e., 2, 20, 200, and 400 ng) on DTC CTC enrichment efficiency (**Fig. S2B**). The optimal amount of TCO-anti-EpCAM was determined to be 200 ng, achieving an efficiency of 90% ± 3% on Click Chips for DTC CTC enrichment. Subsequently, we examined the influence of different quantities of TCO-anti-CD147 (i.e., 1, 10, 100, and 200 ng) on DTC CTC enrichment efficiency (**Fig. S2C**). Click Chips attained the best enrichment efficiency of up to 89% ± 3% when utilizing 100 ng of TCO-anti-CD147. We then compared the enrichment efficiency (**Fig. S2D**) of using the combination of the 200 ng of TCO-anti-EpCAM and 100 ng of TCO-anti-CD147 as an antibody cocktail versus each antibody individually. A remarkable enrichment efficiency of 95% ± 2% was achieved by the dual-antibody cocktail, outperforming the individual antibodies used alone. Finally, we compared the enrichment efficiency of Click Chips with Tz-grafted magnetic beads (**Fig. S2E**) using the same dual-antibody cocktail. The Click Chips

with the dual-antibody cocktail achieved a higher enrichment efficiency of 95% ± 2% compared to 47% ± 6% with the Tz-grafted magnetic bead-based sorting method for enriching DTC CTCs. The enrichment efficiency of Tz-grafted magnetic beads in our study is aligns with that of other magnetic bead-based CTC enrichment methods, which report efficiencies ranging from 40% to 80%, depending on the cell lines and capturing antibodies used in spike-in studies [67-69]. To confirm the consistency of the enrichment efficiency of Click Chips, we evaluated the dynamic range of Click Chips using artificial DTC PBMC samples containing 0 to 400 MDA-T32 cells spiked into samples of 10^6 PBMCs from a female HD (**Fig. S2F**). Here, Click Chips exhibited linear dynamic range of enrichment efficiencies calculated by both DTC CTC cell numbers ($Y = 0.923*X + 2.433$, $R^2 = 0.999$) and the copy numbers of *SRY* transcripts quantified by RT-dPCR in enriched DTC CTCs ($y = 1.169x - 25.27$, $R^2 = 0.982$). Since the MDA-T32 cells are originally derived from a male patient according to American Type Culture Collection (ATCC), and we spiked the male-derived MDA-T32 cells into female HD-derived PBMCs to generate the artificial DTC PBMC samples for this dynamic range study, the *SRY* transcripts that were present in the male-derived MDA-T32 cells and were absent in female HD-derived PBMCs can be used as a specific marker for evaluating the enrichment efficiency. Similarly, the efficiencies of DTC CTC enrichment can also be determined by dividing the copy numbers of *SRY* transcripts quantified by RT-dPCR in DTC CTCs enriched on Click Chips by the copy numbers *SRY* transcripts in MDA-T32 cells initially introduced into the artificial PBMC samples.

2.3 Selection and Validation of a Panel of Seven DTC-specific Genes

After the optimization of DTC CTC enrichment, a panel of seven DTC-specific genes was selected from the Human Protein Atlas dataset and validated using the workflow developed for DTC CTC enrichment by Click Chip + Quantification of the seven DTC-specific genes by RT-dPCR **(Fig. 2A)**. The bioinformatic framework for selecting the panel of seven DTC-specific genes is depicted in **Fig. 2B.** To ensure the genes were highly specific to DTC rather than other tissues, 174 candidate genes were selected from the 13,783 genes found in thyroid gland transcriptome through deep RNA-seq analysis on the basis of elevated expression in the thyroid gland compared 36 different normal tissues in the Human Protein Atlas [70, 71]. 13 Enriched genes were then selected by identifying the genes that displayed at least four-fold

higher expression levels in the thyroid gland than in any other tissue. To enhance specificity, a tissue specificity score (TS) criterion was introduced, which was defined as the fold-change between the expression level in the thyroid gland and that in the second-highest expressing tissue. Choosing genes that have TS $\geq$ 8, eight thyroid-specific genes were selected. To confirm the specificity of the genes to DTC in comparison to other cancers, we conducted further validation in the Cancer Genome Atlas (TCGA) dataset, seven out of these eight genes showed significantly higher expression **(Fig. S3)** in thyroid cancer than in other cancer types (breast invasive carcinoma, colon adenocarcinoma, head and neck squamous cell carcinoma, hepatocellular carcinoma, lung adenocarcinoma, ovarian carcinoma, and prostate adenocarcinoma). Thus, these final seven genes were identified as the panel of seven DTC-specific genes, including Thyroglobulin (*TG*), Thyroid peroxidase (*TPO*), Solute Carrier Family 26 Member 4 (*SLC26A4*), Iodotyrosine Deiodinase (*IYD*), Solute Carrier Family 26 Member 7(*SLC26A7*), Thyroid Stimulating Hormone Receptor (*TSHR*), and Forkhead Box E1 (*FOXE1*) (**Table S1**). Thereafter, we further validated the panel of seven DTC-specific genes using five DTC patient tumor tissues, three thyroid cancer cell lines (i.e., MDA-T32, KTC1, and BCPAP), and three PBMC samples from HDs. The heatmap (**Fig. 2C**) demonstrated that all seven DTC-specific genes exhibited high expression in tumor tissues from DTC patients and were either absent or had low expression in PBMCs from HDs. The dynamic range of RT-dPCR quantification of the DTC-specific genes in DTC CTCs was investigated. DTC CTCs were enriched by Click Chip using the optimized TCO-antibody cocktail (**Fig. S2D**) from the artificial DTC PBMC samples containing 0 to 400 MDA-T32 cells spiked into samples of 10^6 PBMCs. As shown in **Fig. 2D-H**, the dynamic range of RT-dPCR quantification of five out of the seven DTC-specific genes (i.e., *TG, SLC26A4, SLC26A7, TSHR, and FOXE1*) by the workflow (**Fig. 2A**) showed a linear correlation between the number of MDA-T32 cells spiked in PBMCs, and the detected mRNA copies of the five genes (i.e., *TG*, $R^2 = 0.971$; *SLC26A4*, $R^2 = 0.998$; *SLC26A7*, $R^2 = 0.988$; *TSHR*, $R^2 = 0.951$; and *FOXE1*, $R^2 = 0.981$). Since *TPO* and *IYD* were virtually absent in the three thyroid cancer cell lines, we used DTC tissues with confirmed *TPO* and *IYD* expression instead of cell lines to validate the dynamic range of quantification of *TPO* and *IYD* genes. **Fig. 2I-J** showed that there was a positive linear correlation between the amount of DTC tissue-derived total RNA amount and the detected copy numbers of *TPO* ($R^2 = 0.998$) and *IYD* ($R^2 = 0.998$).

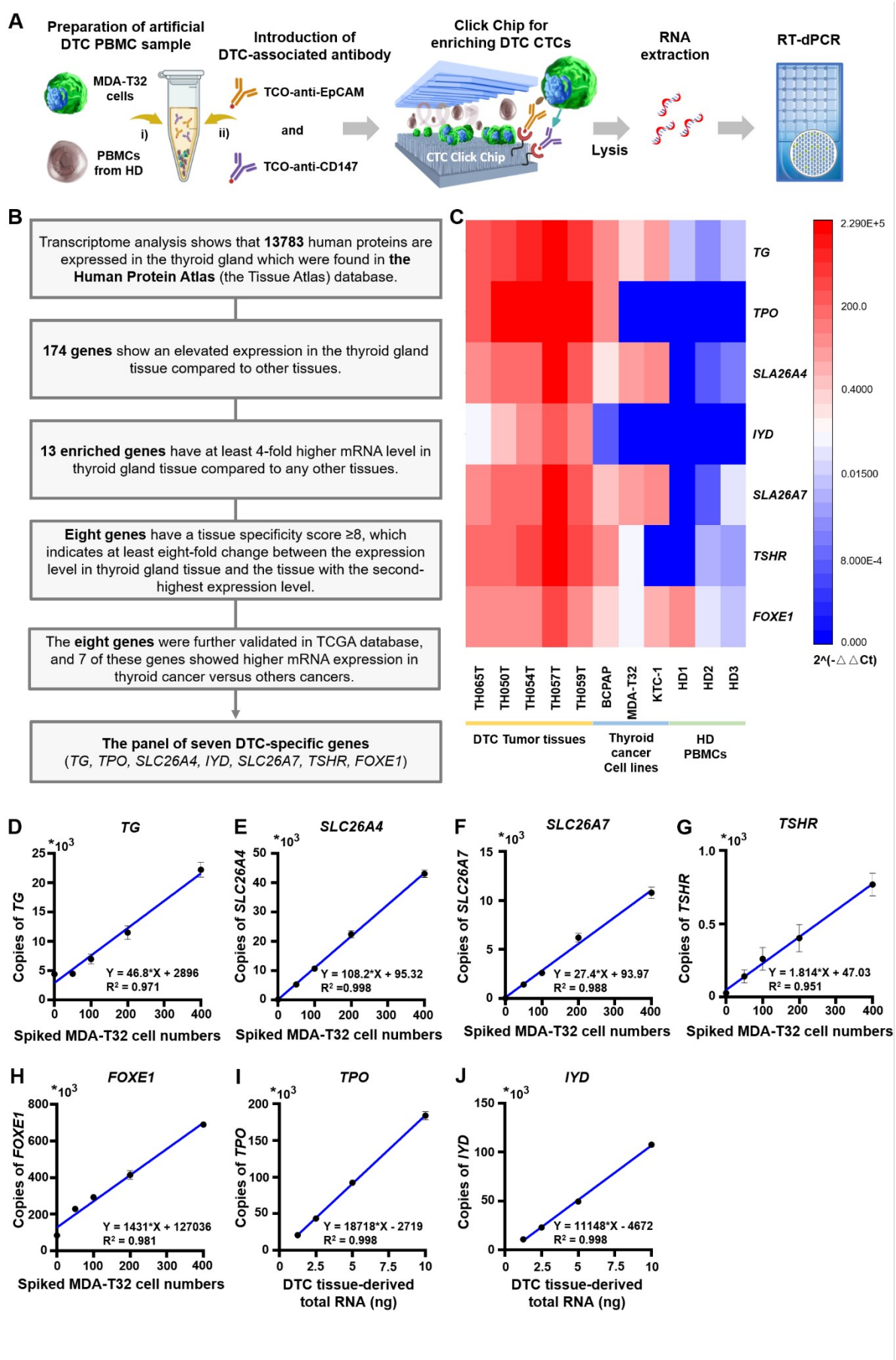
A
Preparation of artificial DTC PBMC sample
MDA-T32 cells
PBMCs from HD
i)
ii)
Introduction of DTC-associated antibody
TCO-anti-EpCAM
and
TCO-anti-CD147
Click Chip for enriching DTC CTCs
CTC Click Chip
Lysis
RNA extraction
RT-dPCR
B
Transcriptome analysis shows that 13783 human proteins are expressed in the thyroid gland which were found in the Human Protein Atlas (the Tissue Atlas) database.
174 genes show an elevated expression in the thyroid gland tissue compared to other tissues.
13 enriched genes have at least 4-fold higher mRNA level in thyroid gland tissue compared to any other tissues.
Eight genes have a tissue specificity score ≥8, which indicates at least eight-fold change between the expression level in thyroid gland tissue and the tissue with the second-highest expression level.
The eight genes were further validated in TCGA database, and 7 of these genes showed higher mRNA expression in thyroid cancer versus others cancers.
The panel of seven DTC-specific genes (TG, TPO, SLC26A4, IYD, SLC26A7, TSHR, FOXE1)
C
TG
TPO
SLA26A4
IYD
SLA26A7
TSHR
FOXE1
2.290E+5
200.0
0.4000
0.01500
8.000E-4
0.000
2^(-△△Ct)
TH065T
TH050T
TH054T
TH057T
TH059T
BCPAP
MDA-T32
KTC-1
HD1
HD2
HD3
DTC Tumor tissues
Thyroid cancer Cell lines
HD PBMCs
D
TG
Copies of TG
Y = 46.8*X + 2896
R² = 0.971
Spiked MDA-T32 cell numbers
E
SLC26A4
Copies of SLC26A4
Y = 108.2*X + 95.32
R² =0.998
Spiked MDA-T32 cell numbers
F
SLC26A7
Copies of SLC26A7
Y = 27.4*X + 93.97
R² = 0.988
Spiked MDA-T32 cell numbers
G
TSHR
Copies of TSHR
Y = 1.814*X + 47.03
R² = 0.951
Spiked MDA-T32 cell numbers
H
FOXE1
Copies of FOXE1
Y = 1431*X + 127036
R² = 0.981
Spiked MDA-T32 cell numbers
I
TPO
Copies of TPO
Y = 18718*X - 2719
R² = 0.998
DTC tissue-derived total RNA (ng)
J
IYD
Copies of IYD
Y = 11148*X - 4672
R² = 0.998
DTC tissue-derived total RNA (ng)

Fig. 2. Selection and validation of the panel of seven DTC-specific genes. (A) Workflow for DTC CTC enrichment by Click Chip + RT-dPCR using artificial DTC PBMC samples. **(B)** A bioinformatic framework was adopted for selecting the panel of seven DTC-specific genes, i.e., *TG*, *TPO*, *SLC26A4*, *IYD*, *SLC26A7*, *TSHR*, and *FOXE1*. **(C)** Heatmap that summarized the expression levels of the seven DTC-specific genes in five DTC tissues, three thyroid cancer cell lines (i.e., MDA-T32, KTC1, and BCPAP), and three PBMC samples from HDs. **(D-H)** Dynamic range of quantification of five out of the seven DTC-specific genes (i.e., *TG*, *SLC26A4*, *SLC26A7*, *TSHR*, and *FOXE1*) by the workflow in **Fig. 2A** using artificial DTC PBMC samples (containing 0-400 MDA-T32 cells). **(I-J)** Dynamic range of RT-dPCR quantification of the remaining two out of seven genes (i.e., *TPO*, and *IYD*) using DTC tissues.

2.4 Quantification of the Panel of Seven DTC-specific Genes in DTC CTCs Enriched by Click Chips

By adopting the optimal DTC CTC enrichment conditions and RT-dPCR analysis, we employed the workflow (**Fig. 3A**) to enrich DTC CTCs from patients' blood samples, followed by quantification of the panel of seven DTC-specific genes in the enriched DTC CTCs. We isolated PBMCs from 59 blood samples collected from 38 newly diagnosed, treatment-naïve DTC patients and 21 HDs. The clinical characteristics of these cohorts are provided in **Table 1** and **Table S2**. Clinical annotation of all the DTC patients was performed by a clinician blinded to the assay. For each blood sample, the PBMCs isolated from 2 mL of aliquoted whole blood were introduced into a Click Chip to enrich DTC CTCs. After RNA extraction, RT-dPCR analysis was carried out to quantify the seven DTC-specific genes, i.e., *TG*, *TPO*, *SLC26A4*, *IYD*, *SLC26A7*, *TSHR*, and *FOXE1*. We summarized the quantification results obtained from 59 blood samples in a heatmap (**Fig. 3B**); the primary copy numbers are log2-transformed for each gene. As shown in the heatmap, higher signals were observed in the DTC cohort, compared with those from the HDs for all DTC-specific genes except for *IYD* and *TPO*. Among the seven DTC-specific genes, four DTC-specific genes (i.e., *TSHR*, *SLC26A7*, *TG*, and *SLC26A4*) showed highly statistically significant differences between DTC patients and HDs ($p < 0.01$), and the results were summarized with a box plot in **Fig. 3C–F**. We then conducted ROC analysis to test the potential of these four DTC-specific genes for distinguishing DTC patients from HDs. The AUROC for distinguishing DTC patients from HDs was ranging from 0.73 to 0.94 for the top four DTC-specific genes, which was 0.94 for *TSHR* (sensitivity = 84%, specificity = 95%), 0.90 for *SLC26A7* (sensitivity = 79%, specificity = 86%), 0.88 for *TG* (sensitivity = 76%, specificity =

90%), and 0.73 for *SCL26A4* (sensitivity = 76%, specificity = 76%), respectively (**Fig. 3G-J**). Data of the other DTC-specific genes for differentiating DTC patients from HDs was summarized in **Fig. S4A-D.** Significantly, we observed that the top three DTC-specific genes demonstrated impressive specificity, each exceeding 85%. This underscored the benefits of using CTC-derived DTC-specific gene quantification for differentiating DTC patients from HDs. No significant differences in the quantifications of DTC-specific genes in DTC CTCs were observed between DTC patients with and without lymph node involvement (**Fig. S5 A-F**), or among DTC patients with different T stages (**Fig. S6 A-F**). Furthermore, in order to confirm the specificity of the DTC-specific genes for differentiating DTC from other cancers, we compared the quantification of seven DTC-specific genes in DTC CTCs from DTC patients (n = 38) to those from patients with other cancers, including ovarian carcinoma (n = 10), prostate adenocarcinoma (n = 10), hepatocellular carcinoma (n = 10), and head and neck squamous cell carcinoma (n = 4) (the clinical characteristics for other cancers were summarized in **Table S3**). As shown in **Fig. S7 A-G**, the quantification of DTC-specific genes in DTC CTCs from DTC patients was significantly higher than in patients with other cancers ($p < 0.05$ for each gene) for all DTC-specific genes except for *IYD*. As summarized in **Fig. S7H-M**, among these DTC-specific genes, AUROC for distinguishing DTC from other cancers was ranging from 0.89 to 0.93 for the top three DTC-specific genes. These results further confirmed the specificity of the top three DTC-specific genes to DTC rather than other cancers. Besides, employing RT-dPCR for the detection and quantification of DTC-specific genes in the enriched DTC CTCs overcomes the low sensitivity commonly encountered with traditional CTC enumeration using microscopy.

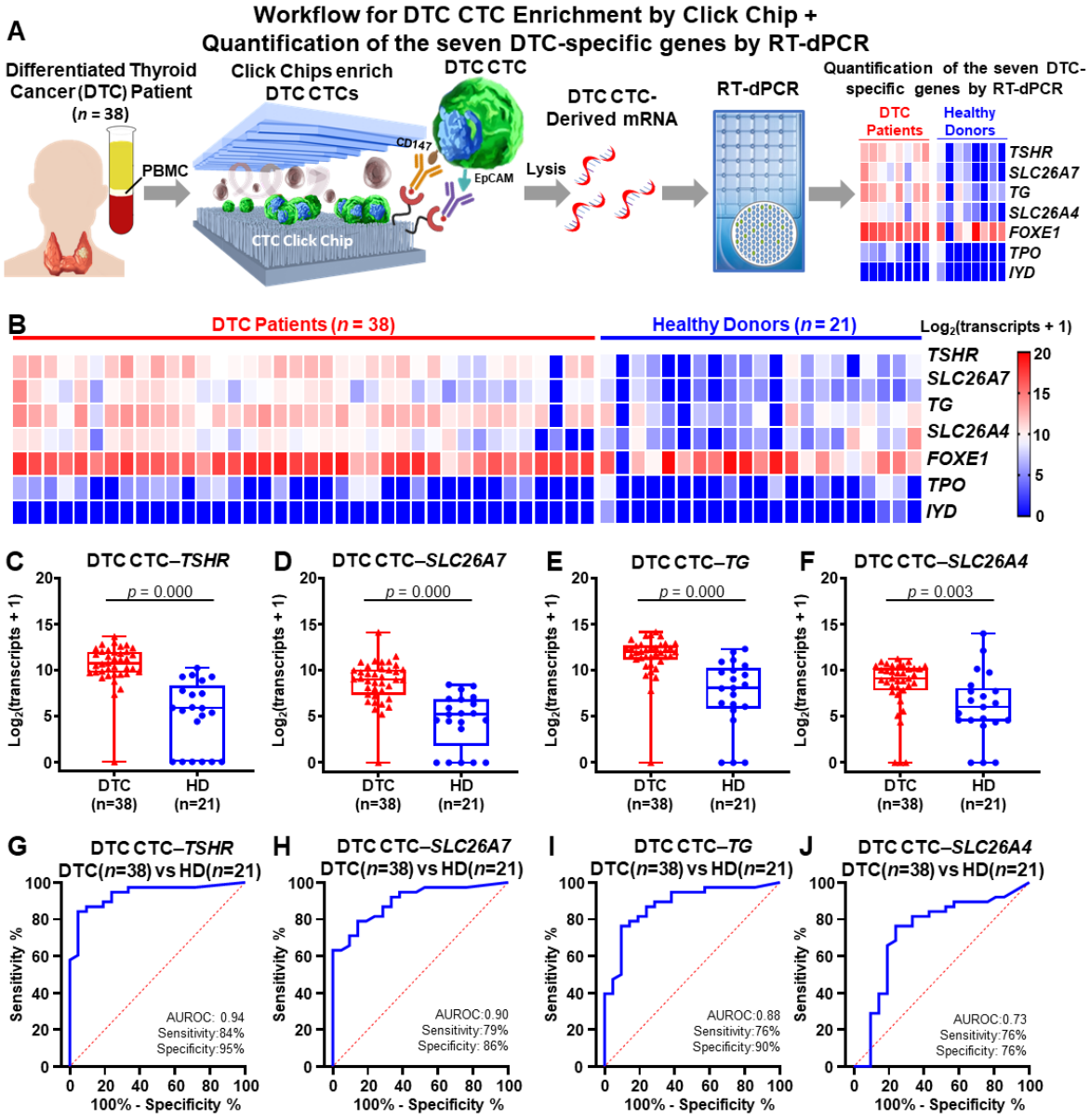

Fig. 3. Quantification of a panel of seven DTC-specific genes in DTC CTCs enriched from patients' PBMC samples. **(A)** Workflow developed for DTC CTC enrichment by Click Chip + Quantification of the seven DTC-specific genes by RT-dPCR using patients' blood samples. **(B)** Heatmaps depicting relative gene expression of each of the seven DTC-specific genes across different patient cohorts, including DTC patients ($n = 38$) and HDs ($n = 21$). Primary copy numbers are $\log_2$-transformed for each gene. **(C-F)** Box plots depicted the four DTC-specific genes (i.e., *TSHR*, *SLC26A7*, *TG*, and *SLC26A4*) with statistically significant differences between DTC patients ($n = 38$) and HDs ($n = 21$). **(G-I)** AUROC of the four DTC-specific genes for differentiating DTC patients ($n = 38$) from HDs ($n = 21$).

2.5 Characterization of DTC ᵗEVs Using Artificial Plasma Samples

To achieve efficient enrichment and characterization of DTC ᵗEVs, we prepared Tz-grafted Click Beads [45], which are capable of enriching TCO-labeled EVs via the click chemistry

reaction between Tz and TCO. To validate the performance of Click Beads for enrichment of DTC tEVs, we generated artificial plasma samples by spiking thyroid cancer cell-derived tEVs (10 μL per sample) into a healthy donor's EV-depleted plasma (90 μL per sample). Here, MDA-T32 cells were cultured in serum-free culture medium, and the DTC tEVs secreted by MDA-T32 cells were harvested by ultracentrifugation and characterized by transmission electron microscopy (TEM), nanoparticle tracking analysis (NTA), and scanning electron microscopy (SEM), following the Minimal Information for Studies of Extracellular Vesicles (MISEV) 2023 guidelines [72] issued by the International Society for Extracellular Vesicle. TEM imaging (**Fig. 4A)** unveiled that MDA-T32 cell-derived tEVs possess characteristic cupped or spherical-shaped morphologies. NTA of MDA-T32 cell-derived tEVs **(Fig. 4B**) indicated an average size of 147.8 ± 65.4 nm and a stock concentration of 9×10^{10} tEVs per mL. Following the workflow developed for click chemistry-mediated enrichment of DTC tEVs using Click Beads (**Fig. 4E,** first two steps), the MDA-T32 cell-derived tEVs were first incubated with TCO-anti-B7H3 and then immobilized onto Tz-grafted Click Beads via the click chemistry reaction between Tz and TCO. SEM was employed to characterize the interfaces between MDA-T32 cell-derived tEVs and Click Beads. SEM image (**Fig. 4C**) showed that multiple TCO-labeled DTC tEVs were immobilized onto a Click Bead. To further confirm the identity of MDA-T32 cell-derived tEVs on Click Beads (in the presence of TCO-anti-B7H3), immunogold staining using anti-CD63 (a universal EV surface marker) was employed to label MDA-T32 cell-derived tEVs. As shown in **Fig. 4D**, MDA-T32 cell-derived tEVs on a Click Bead were successfully labeled with multiple 10 nm gold nanoparticles (AuNPs). We then conducted linearity studies for quantifying $B7H3^+$ DTC tEVs, $MUC1^+$ DTC tEVs, $EpCAM^+$ DTC tEVs, or $CD147^+$ DTC tEVs spiked into the respective artificial plasma by the workflow shown in **Fig. 4E.** Four TCO-grafted antibodies (i.e., TCO-anti-B7H3, TCO-anti-MUC1, TCO-anti-EpCAM, and TCO-anti-CD147) were prepared for enriching different subpopulations of DTC tEVs. Since mRNA encapsulated in DTC tEVs is protected by the lipid bilayer membrane from enzymatic degradation, RT-qPCR quantification of a housekeeping mRNA (β-actin) allows for quantification of enriched DTC tEVs. We prepared artificial plasma samples containing serially diluted tEVs (initial concentration: 9×10^{10} per mL, based on NTA results, Fig. 4B) derived from MDA-T32 cells for the linearity study. Dilution ratios ranged from 1:1 to 1:256. Each of the four TCO-grafted DTC-associated antibodies—TCO-anti-B7H3, TCO-anti-MUC1, TCO-anti-EpCAM, and TCO-anti-CD147—was used in this linearity study. The results (**Fig. 4F–I)** revealed that there was an excellent

linear correlation between the concentrations of spiked DTC tEVs and the β-actin RT-qPCR readouts (B7H3+ DTC tEVs: Y = 1.371*X + 14.18, R^2 = 0.992; MUC1+ DTC tEVs: Y = 1.083.4*X+12.64, R^2 = 0.967; EpCAM+ DTC tEVs: Y = 1.251*X + 12.11, R^2 = 0.993; CD147+ DTC tEVs: Y = 1.024*X + 10.8, R^2 = 0.981).

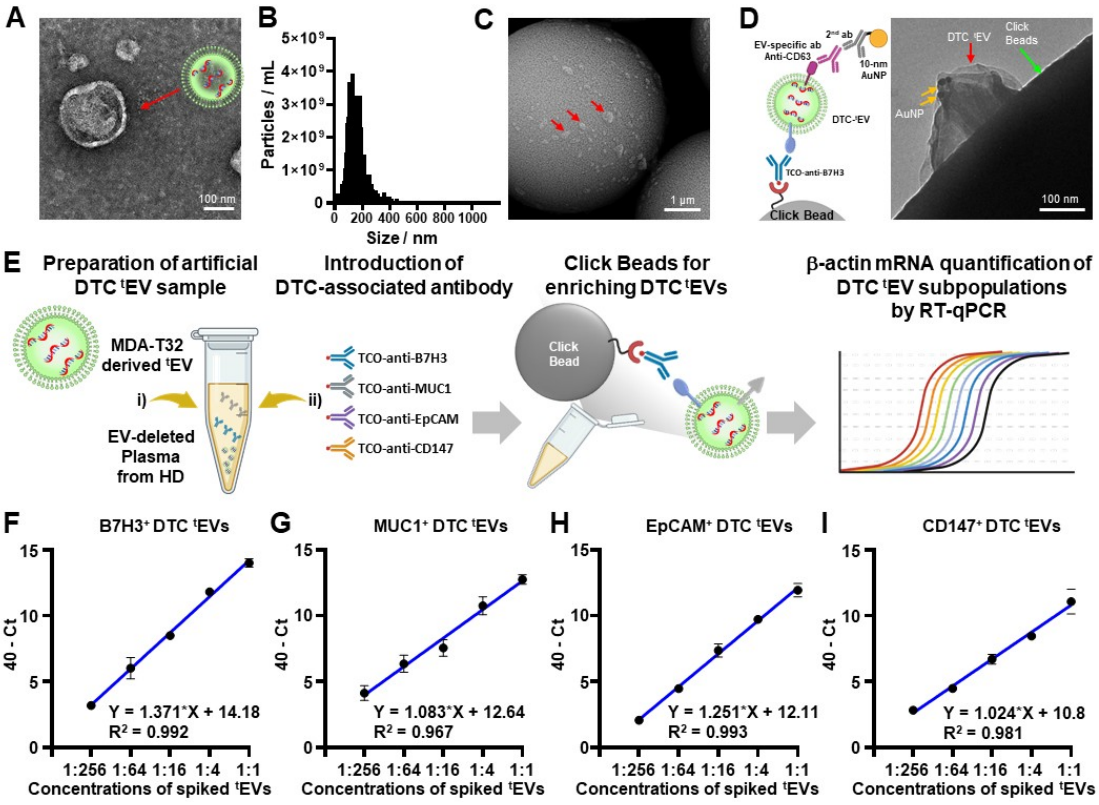

Fig. 4. (A) Characterization of DTC tEVs enriched by Click Beads. (A) A representative transmission electron microscopy (TEM) image (scale bar, 100 nm) of MDA-T32 cell-derived tEVs. **(B)** Size distribution of MDA-T32 cell-derived tEVs measured by nanoparticle tracking analysis (NTA). **(C)** Scanning electron microscopy (SEM) image of MDA-T32 cell-derived tEVs enriched on the surface of Click Beads (scale bar, 1μm). **(D)** A representative TEM image of MDA-T32 cell-derived tEVs enriched on a Click Bead after immunogold staining by anti-CD63-grafted gold nanoparticles. **(E)** Workflow developed for DTC tEV enrichment by Click Beads + β-actin mRNA quantification by RT-qPCR. Four TCO-grafted DTC-associated antibodies (i.e., TCO-anti-B7H3, TCO-anti-MUC1, TCO-anti-EpCAM, or TCO-anti-CD147) were employed for enriching four different subpopulations of DTC tEVs. **(F-I)** Dynamic range of RT-qPCR quantification of β-actin mRNA expression for the four subpopulations of DTC tEVs (i.e., B7H3+ DTC tEVs, MUC1+ DTC tEVs, EpCAM+ DTC tEVs, and CD147+ DTC tEVs) by the workflow (DTC tEVs Enrichment by Click Beads + β-actin mRNA Quantification by RT-qPCR) using MDA-T32 derived tEV-spiked artificial plasma samples.

2.6 Quantification of Subpopulations of DTC ᵗEVs Using Clinical Plasma Samples Collected from DTC Patients and Healthy Donors

After confirming the linearity for detecting different subpopulations of DTC ᵗEVs, we adopted the workflow in **Fig. 5A** for quantification of the four subpopulations of DTC ᵗEVs (i.e., B7H3$^+$ DTC ᵗEVs, MUC1$^+$ DTC ᵗEVs, EpCAM$^+$ DTC ᵗEVs, and CD147$^+$ DTC ᵗEVs) using clinical plasma samples collected from DTC patients and HDs. To test our hypothesis that elevated subpopulations of DTC ᵗEVs can be detected in DTC patients rather than in HDs, we first conducted a pilot study using plasma samples of eight DTC patients and eight HDs. Each of the four DTC ᵗEV subpopulations was quantified by RT-qPCR, and the quantification results were summarized in **Fig. S8 A-D.** Three out of four subpopulations of DTC ᵗEVs (i.e., B7H3$^+$ DTC ᵗEVs, MUC1$^+$ DTC ᵗEVs, and EpCAM$^+$ DTC ᵗEVs) exhibited potential capabilities to distinguish DTC patients from HDs ($p < 0.05$), and were therefore selected for subsequent studies using a larger clinical cohort, including an additional 30 DTC patients and 13 HDs. The clinical characteristics of the overall 38 DTC patients across all stages and 21 HDs were summarized in **Table 1 and Table S2**. Clinical annotation of all the plasma samples was performed by a clinician blinded to the assay. For each clinical sample, we employed the aforementioned workflow (**Fig. 5A**), and the quantification results that presented as 40-Ct values for the selected three subpopulations of DTC ᵗEVs were summarized in a heatmap (**Fig. 5B**). As shown in the heatmap, higher signals were observed in the DTC cohort, compared with those from the HDs for all three subpopulations of DTC ᵗEVs. As depicted in **Fig. 5C-E**, the β-actin mRNA expression levels of all three DTC ᵗEV subpopulations were significantly higher ($p < 0.01$) in DTC patients compared to HDs, with AUROCs of 0.91 (sensitivity = 89%, specificity = 81%) for B7H3$^+$ DTC ᵗEVs, 0.87 (sensitivity = 95%, specificity = 67%) for MUC1$^+$ DTC ᵗEVs, and 0.76 (sensitivity = 71%, specificity = 76%) for EpCAM$^+$ DTC ᵗEVs, respectively (**Fig. 5F-H**). We observed that the top two DTC ᵗEV subpopulations showed high sensitivity. No significant differences in the quantifications of DTC ᵗEV subpopulations were observed between DTC patients with and without lymph node involvement (**Fig. S9 A-C**), or among DTC patients with different T stages (**Fig. S10 A-C**). This suggested that utilizing Click Beads and RT-qPCR for the quantification of DTC ᵗEV subpopulations held promise for developing a sensitive assay for distinguishing DTC patients from HDs.

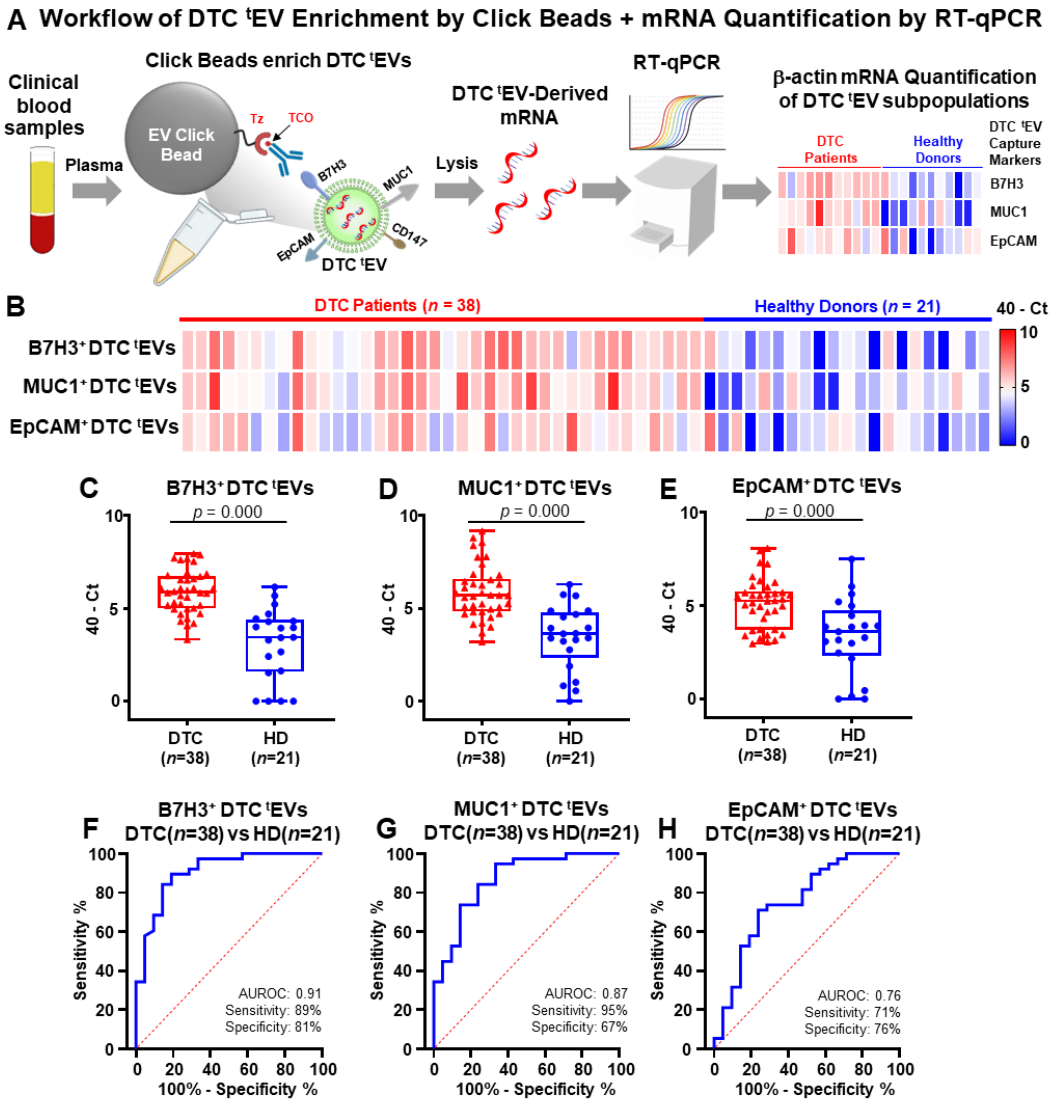

Fig. 5. Quantifying the selected three subpopulations of DTC ᵗEVs (i.e., B7H3⁺ DTC ᵗEVs, MUC1⁺ DTC ᵗEVs, and EpCAM⁺ DTC ᵗEVs) using clinical plasma samples. (A) Workflow for subpopulations of DTC ᵗEV enrichment by Click Beads, followed by β-actin mRNA quantification using RT-qPCR. **(B)** Heatmaps summarizing RT-qPCR readouts of plasma samples from DTC patients (n = 38, across all stages) and HDs (n = 21). **(C-E)** Significantly higher quantities of subpopulations of B7H3⁺ DTC ᵗEVs, MUC1⁺ DTC ᵗEVs, and EpCAM⁺ DTC ᵗEVs were observed in DTC patients (n = 38) compared to those for HDs (n = 21). **(F-H)** AUROC of DTC ᵗEV subpopulations that were calculated using 40-Ct values for B7H3⁺ DTC ᵗEVs, MUC1⁺ DTC ᵗEVs, and EpCAM⁺ DTC ᵗEVs for detecting DTC patients (n = 38) from HDs (n = 21).

2.7 The Combined DTC CTC/ᵗEV Assay for DTC Detection

The outstanding diagnostic specificity shown by the DTC CTC-derived gene signature (**Fig. 3**) and superb diagnostic sensitivity demonstrated by the quantitative readouts of subpopulations of DTC ᵗEVs (**Fig. 5**), prompted us to synergistically combine them. To

achieve satisfactory diagnostic performance in differentiating DTC patients from HDs, we initially tried various combinations of the Combined DTC CTC/tEV Assay. This involved integrating the three most significant DTC-specific genes in DTC CTCs, each with specificity over 85% (i.e., DTC CTC-*TSHR*, DTC CTC-*SLC26A7*, DTC CTC-*TG*), and the two most significant DTC tEV subpopulations (i.e., $B7H3^+$ DTC tEVs, $MUC1^+$ DTC tEVs), each with sensitivity over 85%. The AUROCs for different combinations were summarized in **Table S4**. As a result, the top-performing gene, DTC CTC-*TSHR* and the most significant DTC tEV subpopulation, $B7H3^+$ DTC tEVs were selected as the best combination for the Combined DTC CTC/tEV Assay. The DTC CTC-*TSHR* and $B7H3^+$ DTC tEVs were complementary in terms of sensitivity and specificity and were combined into a single metric score named Combined DTC CTC/tEV Score using a logistic regression model **(Fig. 6A)** for detecting DTC.

Combined DTC CTC/tEV Score defined as:

$$Combined\ DTC\ CTC/^{t}EV\ Score = \text{¿}$$

$$-8.682 + 0.005 * [DTC\ CTC - TSHR] + 1.385 * \text{¿}$$

As depicted in the box plot **(Fig. 6B)**, the Combined DTC CTC/tEV Score of the DTC cohort (n = 38) was significantly higher ($p < 0.01$) than the HD cohort (n = 21). Then, ROC analysis was performed to test the potential of the Combined DTC CTC/tEV Score for distinguishing DTC patients from HDs. The AUROC of the Combined DTC CTC/tEV Score was 0.99 (95% CI, 0.96–1.00; sensitivity = 95%, specificity = 95%, **Fig. 6C**), which demonstrated excellent diagnostic performance for differentiating DTC patients from HDs. We used Click Chips for CTC enrichment in this study, employing conventional and well-validated CTC capturing markers, i.e., EpCAM and CD147. The Click Chips with this dual-antibody cocktail achieved a high enrichment efficiency of 95% ± 2%. Click Chip leverages click chemistry-mediated CTC enrichment and the "NanoVelcro" cell-affinity substrates, which utilize Velcro-like topographic interactions between the nanostructured substrates and the microvilli of CTCs. This method is ideal for CTC mRNA quantifications due to its rapid, efficient, and specific enrichment of CTCs. The downstream gene profiling of the enriched CTCs using DTC CTC-specific gene panel can reflect the heterogeneity of CTCs. However, due to the small number of antigens on each tEV and insufficient interactions between the tEV antigens and the capture

antibodies, tEV enrichment typically shows suboptimal performance if capturing markers are not well-selected and combined. Additionally, tEVs comprise heterogeneous subpopulations. To tackle this challenge, we incorporated two additional capturing markers along with the conventional CTC capturing markers, using click chemistry-mediated tEV enrichment technologies, specifically Click Beads. Our results demonstrated that among the four capturing markers for tEVs, targeting B7H3 and MUC1 showed optimal enrichment efficiency for tEVs. Click Beads can be produced in large quantities and are amenable to automation, making them suitable for high-throughput EV enrichment applications. Chip-based assays and Bead-based assays are commonly utilized techniques for the enrichment and analysis of CTCs and EVs originating from different types of tumors. The widespread adoption of Chip-based assays or hybrid of chip- and bead-based assay for CTC enrichment can be mainly attributed to i) their compatibility with an FDA-cleared method (CellSearch®), ii) the larger size of CTCs (typically 10–30 μm compared to 100–1000 nm for EVs), and iii) their capability for high-throughput processing of rare CTCs from substantial volumes of biofluid. On the other hand, Bead-base assays are more favored for EV enrichment due to the high abundance of EVs (approximately 10^{10} EVs/mL plasma compared to less than one CTC/mL plasma), necessitating a relatively smaller volume of biofluid. These assays have shown various clinical applications, such as early detection, treatment monitoring, and prognosis of solid tumors, each accompanied by its own set of advantages and disadvantages (summarized in **Table S5**).

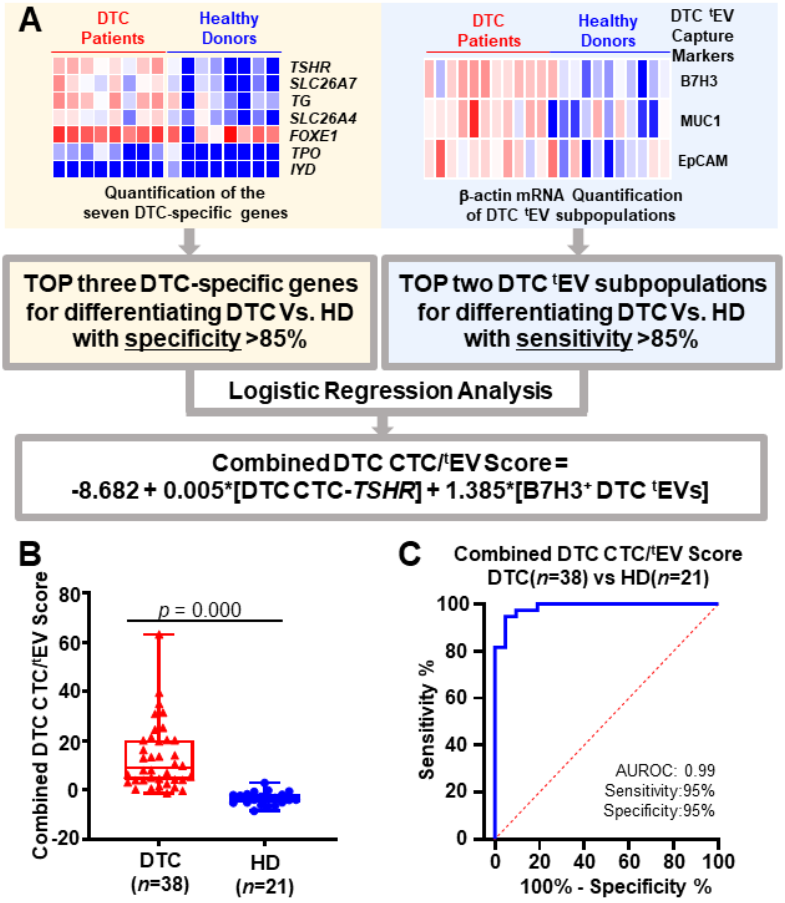

Fig. 6. The Combined DTC CTC/ᵗEV Assay for DTC detection. (A) A workflow of how the Combined CTC/ᵗEV Score was calculated. The top-performing DTC CTC–*TSHR* and B7H3⁺ DTC ᵗEVs were integrated into Combined DTC CTC/ᵗEV Score using a logistic regression model for differentiating DTC patients (n = 38) from HDs (n = 21). **(B)** Box plots showed that DTC group has significantly higher Combined DTC CTC/ᵗEV Score than the HD group. **(C)** The Combined DTC CTC/ᵗEV Score demonstrated excellent diagnostic performance for differentiating DTC patients from HDs with an AUROC of 0.99 (sensitivity = 95%, specificity = 95%).

3. Conclusion

We have successfully demonstrated and validated the Combined DTC CTC/ᵗEV Assay, effectively utilizing the synergistic roles of the two liquid biopsy components – CTCs and ᵗEVs – for non-invasive detection of DTC, a typically indolent tumor. By integrating the excellent sensitivity of ᵗEVs and impressive specificity of CTCs, this assay shows remarkable diagnostic accuracy for detecting DTC with an AUROC of 0.99, along with high sensitivity (95%) and specificity (95%), surpassing the performance of individual DTC CTC or DTC ᵗEV alone. To overcome the limitations in sensitivity and specificity of traditional immunoaffinity-based CTC/ᵗEV enrichments and to accommodate tumor heterogeneity, our assay incorporates click chemistry-mediated enrichment. This method combines two Tz-functionalized

platforms: CTC Click Chips for DTC CTC enrichment and tEV Click Beads for DTC tEV enrichment, alongside a series of TCO-grafted DTC-associated antibodies. The workflow depicted in **Fig. 1** maximizes the use of patient blood samples by simultaneously testing PBMCs and plasma. PBMCs are enriched for DTC CTCs via click chemistry, followed by RT-dPCR to quantify seven DTC-specific gene signatures. Concurrently, plasma samples undergo click chemistry-mediated DTC tEV enrichment, quantifying three DTC tEV subpopulations by RT-qPCR. The resultant data were used to calculate Combined DTC CTC/tEV Scores for distinguishing DTC patients from HDs. Significantly, this approach capitalizes on the complementary diagnostic roles of DTC CTCs and DTC tEVs. While DTC CTCs (sometimes elusive in early-stage indolent tumors) confer specificity, DTC tEVs (detectable early and persisting through all stages) ensure the assay's sensitivity. This work represents the continuous development and integration of nanomaterials-embedded liquid biopsy technologies to address unmet clinical needs in the field of thyroid cancer. A major paradigm shift in thyroid cancer care has been the adoption of thyroid lobectomy instead of total thyroidectomy as initial surgical management for localized DTC. By preserving half of the thyroid lobe, this allows some patients to avoid lifelong thyroid hormone supplementation, reduces risk of nerve injury by 50%, and completely negates the risk of hypoparathyroidism. However, the lack of availability of a thyroid cancer biomarker to detect cancer recurrence in patients with a remaining thyroid lobe leads many patients and physicians to choose total thyroidectomy over thyroid lobectomy. Thus, the Combined DTC CTC/tEV Assay may allow patients to avoid unnecessary overtreatment of thyroid cancer in the future.

Our study introduces a novel dual-enrichment approach using click chemistry to simultaneously isolate and analyze DTC CTCs and tEVs from the same blood sample, enhancing liquid biopsy diagnostics. Additionally, we implement digital scoring of DTC CTCs using a DTC-specific panel from a bioinformatic framework, offering detailed insights into molecular characteristics. Furthermore, our detection of specific subpopulations of DTC tEVs provides deeper understanding of tEV heterogeneity and their role in thyroid cancer, advancing the field significantly.

4. Experimental Section

Thyroid cancer cell lines

Three thyroid cancer cell lines including MDA-T32, KTC1, and BCPAP were purchased from ATCC and cultured using RPMI-1640 growth medium with 10% fetal bovine serum, 1% L Glutamine, and penicillin-streptomycin (100 U ml^{-1}) (Thermo Fisher Scientific) in a humidified incubator with 5% CO_2.

Immunofluorescent staining for EpCAM, CD147, B7H3, and MUC1 Expression on Thyroid Cancer Cell Lines

To test the expression of the surface makers, i.e., EpCAM, CD147, B7H3, and MUC1 on thyroid cancer cell lines, three thyroid cancer cell lines, i.e., MDA-T32, KTC1, and BCPAP were employed for the immunocytochemistry (ICC) staining using the following protocol. First, the cultured cells were harvested and smeared onto glass slides, then the glass smears were fixed with 4% paraformaldehyde fixative solution (Electron Microscopy Sciences) for 10 min and were subsequently incubated with 0.1% Triton X-100 for 10 min at room temperature. Next, these cells were incubated overnight at 4 °C with one of the four primary antibodies, namely monoclonal mouse IgG human EpCAM antibody (1:100 v/v, R&D systems), monoclonal mouse IgG human CD147 antibody (1:100 v/v, R&D systems), monoclonal mouse IgG human B7H3 antibody (1:100 v/v, BioLegend), or monoclonal mouse IgG human MUC1 antibody (1:100 v/v, R&D systems), in a 200 µL of phosphate-buffered saline (PBS) solution containing 2% donkey serum (Jackson ImmunoResearch). After rinsing with PBS, these cells were incubated with the secondary antibody, the donkey anti-Mouse IgG (H+L) (Alexa Fluor™ 488, 1:500 v/v; Invitrogen), in a 200 µL of PBS solution containing 2% donkey serum at room temperature for 45 min. After rinsing with PBS, these cells were treated with DAPI solution (1:1000 v/v, Invitrogen) for nuclear staining. Thereafter, these cells were imaged using a 40× objective lens on a Nikon Eclipse 90i fluorescence microscope.

Fabrication of Click Chips

SiNWS with vertical alignment were fabricated via a process that integrates photolithographic patterning and silver (Ag) nanoparticle-templated wet etching, following the workflow detailed in our previous publications [73]. In brief, a (100) p-type silicon wafer (Silicon Quest

International) with a resistivity of approximately 10 to 20 Ω·cm was served as the substrate to deposit a thin-film photoresist (AZ 5214, AZ Electronic Materials USA Corp.) through spin-coating. Following exposure to UV light, the silicon wafer was immersed into the etching solution containing hydrofluoric acid (4.6 M; Sigma-Aldrich), silver nitrate (0.2 M; Sigma-Aldrich), and deionized water. Subsequently, the silicon wafer underwent a 15-minute immersion in boiling aqua regia to remove the silver film. The resulting SiNWS exhibited a length of approximately 10 μm. The SiNWS underwent multiple rinses with acetone (≥ 99.5%; Sigma-Aldrich) and anhydrous ethanol (Sigma-Aldrich) to eliminate the patterned photoresist. A Tz motif was incorporated onto chip surfaces via two-step chemical modification method. (i) Surface salinization: the SiNWS were positioned within a Teflon frame in a glass beaker and subjected to incubation with a piranha solution for 1 hour. Following successive rinses with deionized water and ethanol three times, the SiNWS were dried with nitrogen gas. The SiNWs were then sealed within a vacuum desiccator and exposed to silane vapor of (3-aminopropyl) triethoxysilane (200 μL; Sigma-Aldrich) for 45 min to introduce amine groups onto the SiNWS. (ii) To graft Tz motifs onto SiNWS, freshly prepared SiNWS-NH_2 were reacted with methyltetrazine-PEG4-NHS ester (0.32 mg; BroadPharm) in PBS (200 μL) for 1 hour. The functionalized Tz-grafted SiNWS were then rinsed with PBS three times before being employed in DTC CTC enrichment experiments.

Preparation of TCO-grafted DTC-associated antibody conjugates

The TCO-grafted DTC-associated antibody conjugates (i.e., TCO-anti-EpCAM, TCO-anti-CD147, TCO-anti-B7H3, or TCO-anti-MUC1) were produced by incubating TCO-PEG_4-NHS ester (4 μM, Click Chemistry Tools) with each of the 4 antibodies (i.e., anti-EpCAM, anti-CD147, anti-B7H3, and anti-MUC1) in PBS solution (pH 7.4) at room temperature for 30 min according to previously optimized conditions [74]. Excess TCO-PEG_4-NHS was purified by Zeba 40 kDa column. The resultant TCO-antibody conjugates (100 μg mL^{-1}) in PBS solution were aliquoted and stored at –20 °C until use.

Preparation of artificial DTC PBMC samples

To enable subsequent cell imaging and counting during the optimization process, cultured MDA-T32 cells (1×10^6 ml^{-1}) were pre-stained with a Vybrant DiD red fluorescent dye (Invitrogen) in serum-free culture medium at 37 °C for 1 hour. PBMCs were isolated from a

HD with approval from the University of California, Los Angeles Institutional Review Board (IRB#19-000857). Excess cell-labeling dye was removed by centrifuging the labeled suspension at 1500 rpm for 5 min and then rinsed with PBS twice. Typical artificial DTC PBMC samples were prepared by spiking the pre-stained MDA-T32 cells into the PBMCs (5 × 10^6 cells ml^{-1}) in 200 μL of RPMI 1640 solution. The artificial PBMC samples were later used during the optimization of DTC CTC enrichment using Click Chips.

Optimization of DTC CTC enrichment using Click Chips

For DTC CTC enrichment, PBS (200 μL) was first introduced into a Click Chip via a digital fluidic handler at a flow rate of 4 ml $hour^{-1}$ to confirm that an appropriate seal was made between the patterned PDMS chaotic mixer and the Tz-grafted SiNWS. The artificial DTC PBMC samples were incubated with TCO-anti-EpCAM (i.e., 2, 20, 200 and 400 ng, respectively) or TCO-anti-CD147 (i.e., 1, 10, 100 and 200 ng, respectively) in RPMI 1640 (200 μl) at room temperature for 30 min and then centrifuged at 300g for 10 min to remove the excess TCO-anti-EpCAM/CD147 and nonreactive TCO-PEG4-NHS ester. Then the samples were resuspended in 200 μL PBS and infused into Click Chips at the previously optimized flow rate of 0.5 mL $hour^{-1}$ [66, 75]. For DTC CTC enumeration, the DTC CTCs enriched in the Click Chips were fixed with 4% Paraformaldehyde in PBS (200 μL) and then stained with DAPI for imaging under a Nikon 90i fluorescence microscope. To compare the enrichment efficiency of Click Chips with magnetic beads, the bioorthogonal ligation-mediated DTC CTC enrichment on Tz-grafted magnetic beads was carried out using the DiD pre-stained artificial DTC PBMC samples and TCO-grafted DTC-associated antibody cocktail (TCO-anti-EpCAM and TCO-anti-CD147) in the same quantities used with Click Chips. For the DTC CTC enrichment comparison, the Dynabeads™ M-270 Amine (2 × 10^8 beads, 100 μL, Thermo Fisher Scientific) were reacted with Tz-sulfo-NHS ester (0.32 mg, 3.8 mM) in PBS buffer for 1 h to produce the Tz-grated magnetic beads. The Tz-grafted magnetic beads were incubated with the TCO-grafted DTC PBMC samples at room temperature for 30 min. Then the DTC CTC-enriched magnetic beads were stained with DAPI and imaged under the Nikon 90i fluorescence microscope.

Validation of 7 DTC-specific genes

The selected panel of 7 DTC-specific genes were validated using DTC tissues, thyroid cancer cell lines (i.e., MDA-T32, KTC1, and BCPAP), and HD BPMCs. Total RNA was extracted from the DTC tissues, thyroid cancer cell lines, and PBMCs from HDs using the Qiagen (Dusseldorf, Germany) Rneasy kit. Then the complementary DNA (cDNA) was synthesized using a Thermo Scientific Maxima H Minus Reverse Transcriptase Kit according to the manufacturer's protocols. The 7 DTC-specific gene transcripts (i.e., *TG*, *TPO*, *SLC26A4*, *IYD*, *SLC26A7*, *TSHR*, and *FOXE1*) were tested for each sample using RT-qPCR. Predesigned Taqman assays (Thermo Fisher Scientific) containing primers and probes for each gene (**Table S6**) were used in the RT-qPCR, which was conducted on a CFX Duet Real-Time PCR System (Bio-Rad, USA) following the manufacturer's protocols.

Linearity studies for the 7 DTC-specific gene quantification

The DTC CTCs enriched by Click Chips according to the protocol depicted in **Fig. 3A** were lysed with 600 µL Trizol (ZYMO Research) and 600µL ethyl alcohol. RNA was extracted using a Direct-zol™ RNA Microprep Kit (ZYMO Research, USA) according to the manufacturer's instructions. Then, the cDNA was synthesized using a ThermoFisher Scientific Maxima H Minus First Strand cDNA Synthesis Kit according to the manufacturer's instructions. For the optimization and linearity studies, cDNA was tested for *SRY* transcripts and the 7 DTC-specific genes (i.e., *TG*, *TPO*, *SLC26A4*, *IYD*, *SLC26A7*, *TSHR*, and *FOXE1*) using RT-dPCR. For RT-dPCR, the reaction mixture (40 µL) including 4 µL of pre-amplified product was loaded into each well of a nanoplate (26 K, 24 wells). The nanoplate was transferred into the QIAcuity instrument (Qiagen, Germany) for the following PCR process. A programmed Thermal Cycler was set at 95°C for 2 min followed by 40 cycles of 95 °C for 15 s and 60 °C for 30 s. The readouts of positive and negative partitions were counted automatically by the instrument and analyzed via QIAcuity software. For the dynamic range of RT-dPCR quantification of five out of seven DTC-specific genes (i.e., *TG*, *SLC26A4*, *SLC26A7*, *TSHR*, and *FOXE1*) by the workflow (DTC CTC enrichment by Click Chip + Quantification of DTC-specific genes by RT-dPCR, **Fig. 2A**), the artificial DTC PBMC samples (Contain 0 – 400 MDA-T32 cells) were enriched by Click Chips using optimized conditions. After total RNA was extracted and then cDNA synthesized, the quantification of the 5 DTC-specific genes that were highly expressed in thyroid cancer cell lines was performed by RT-dPCR. The DTC tissue-derived total RNA with serial dilution (i.e., 2.5, 5, 7.5, and 10 ng, respectively) was directly used for testing the dynamic range of RT-dPCR

quantification of the other two DTC-specific genes (i.e., TPO and IYD) that were not expressed in thyroid cancer cell lines.

Study Cohort

All the DTC patients in this study were enrolled between October 2019 and October 2023 at Ronald Reagan UCLA Medical Center. All the participants were at least 18 years of age. Treatment-naïve DTC patients across all stages ($n = 38$) were enrolled in this study. Cancer patients who had second malignant tumors or severe mental diseases were excluded. The control cohorts consisted of HDs ($n = 21$) and other cancers including ovarian carcinoma (n = 10), prostate adenocarcinoma (n = 10), hepatocellular carcinoma (n = 10), and head and neck squamous cell carcinoma (n = 4). A detailed description of each cohort and clinical characteristics can be found in the Supplementary Information (Supplementary Tables S2 and S3). All patients and healthy donors provided written informed consent for this study according to the IRB protocols (IRB #19-000 857, #10-000727) at UCLA and (IRB #00000066) at Cedars-Sinai Medical Center. None of the enrolled patients was a part of any clinical trial. Patient allocation to each of the cohorts was not random and was defined by their clinical diagnosis.

Clinical Blood Sample Processing to obtain plasma and PBMCs

Peripheral venous blood samples were collected from patients with DTC and other cancers as well as HDs. Each 8 mL of blood sample was collected in a BD Vacutainer plastic tube (BD, Cat. #366 643) with EDTA. Plasma samples were isolated first and then PBMCs were isolated from blood cells within 4.0 hrs of blood collection. The plasma samples were collected after centrifugation at 500 g for 10 min, followed by the second centrifugation at 4600 g for 10 min. The final plasma samples were then aliquoted and stored in -80 °C refrigerators before use. Human peripheral blood mononuclear cells (PBMCs) were separated by gradient centrifugation with Lymphoprep (Stemcell, USA) and SepMate^{TM}–50 (Stemcell, USA) using the manufacturer's protocol. The obtained PBMCs were suspended in Bambanker serum-free cell freezing medium (FUJIFILM, Japan), which were subsequently aliquoted into labeled cryovials at the volume equivalent to 2mL of whole blood and banked in liquid Nitrogen (under -180 °C). At the time of experimentation, 2-mL whole blood equivalency of samples

was retrieved and immediately thawed in a 37 °C water bath. After rinsing with PBS, the PBMCs were re-suspended in 200 μL of PBS for DTC CTC enrichment.

Quantification of 7 DTC-specific genes in DTC CTCs enriched by Click Chips using clinical samples

PBMCs isolated from each clinical sample collected from DTC patients, HDs, and other cancers were re-suspended in 200μL of PBS and incubated with the cocktail of TCO-anti-EpCAM (200 ng) and TCO-anti-CD147 (100 ng) in RPMI 1640 (200 μL) at room temperature for 30 min and then centrifuged at 300 g for 10 min to remove the supernatant. Then the pellets were washed and resuspended in 200 μL PBS and injected into Click Chips at the optimal flow rate of 0.5 ml h^{-1}. The DTC CTCs enriched on the Click Chips were lysed with 600 μL Trizol (ZYMO Research) and 600 μL ethyl alcohol. Total RNA was extracted for each sample and RT-dPCR was performed to quantify the 7 DTC-specific genes using the same protocol as described above for the linearity studies.

Collection of DTC ^{t}EVs from Cell Culture Supernatant

DTC cell line of MDA-T32 was cultured in 18 dishes (Thermo Scientific Nunc EasYDish Dishes) under standard conditions until reaching 70 - 80% of confluency. Next, cells were cultured with an exosome-production culture medium (13 mL per dish) for 24 h. A total of 234 mL conditional medium was collected and centrifugated at 300 g, 4 °C for 10 min followed by another centrifugation step at 2800 g, 4 °C for 10 min to discard cell debris. The resulting culture medium was carefully transferred to Ultra-Clear Tubes (38.5 mL, Beckman Coulter, Inc., USA) and was then ultracentrifuged at 100 000 g, 4 °C for 120 min. The enriched DTC ^{t}EVs were suspended in 400 μL PBS and aliquoted as original DTC ^{t}EV samples.

Fabrication of Click Beads

The 5 μm silica microbeads (10 mg) underwent acid incubation (2.0 N HCl, 10 min) to regenerate hydroxyl groups. Subsequently, they were immediately silanized in an ethanol solution (600 μL) containing 4% (3-aminopropyl) triethoxysilane (25 μL) for 45 min at room temperature. The amine-functionalized silica microbeads were rinsed three times with ethanol

to eliminate unbound silane and then subjected to a reaction with methyltetrazine-PEG-NHS ester (0.94 mg) in DMSO/PBS (pH = 9.0, 600 μL) for 60 min.

DTC ᵗEVs enrichment from artificial plasma samples and clinical plasma samples

For the artificial plasma samples, each 10 μL aliquot of the DTC ᵗEVs pellets (initial concentration: 9×10^{10} per mL, based on NTA results) was introduced into 90 μL of EV-depleted HD's plasma with a serial dilution of the spiked MDA-T32 cell-derived ᵗEVs ranging from 1:1, 1:4, 1:16, 1:64, to 1:256. Additionally, 90 μL of healthy donor's EV-depleted plasma spiked with 10 μL of PBS was used as a negative control. For clinical plasma samples, each 100 μL plasma sample was centrifuged at 10,000 g for 10 min after immediate thawing in 37 °C water bath. Then 100 ng of each TCO-grafted DTC-associated antibody (i.e., TCO-anti-EpCAM, TCO-anti-CD147, TCO-anti-B7H3, or TCO-anti-MUC1) were mixed with the artificial or clinical plasma samples for 45 min at room temperature to obtain TCO-grafted DTC ᵗEVs plasma samples. The resulting samples were then incubated with Click Beads for 45 min followed by a centrifugation at 13,000 g for 1.5 min to remove the supernatant, followed by rinsing the Click Beads with enriched DTC ᵗEVs three times using PBS. Finally, the DTC ᵗEVs were quantified by measuring the β-actin mRNA levels using one-step RT-qPCR.

Quantification of β-actin mRNA from enriched DTC ᵗEVs by RT-qPCR

The enriched DTC ᵗEVs on Click Beads were lysed using 10 μL XpressAmp™ Lysis Buffer containing 1% Thioglycerol (Promega, USA). Then, the lysed products were incubated at room temperature for 10 min with gentle shaking at 40 - 50 rpm. The collected sample lysate was subjected to one-step RT-qPCR using a PrimeDirect™ Probe RT-qPCR Mix (Takara, Japan), along with β-actin primers and probes for DTC ᵗEV quantification by a CFX Duet Real-Time PCR System (Bio-Rad, USA). A programmed Thermal Cycler was set at 90 °C for 3 min and 60 ℃ for 5 min followed by 45 cycles of 95 °C for 15 s and 60 °C for 30 s.

TEM Characterization of DTC ᵗEVs

The DTC ᵗEVs, either in solution or enriched onto Click Beads, were fixed in 4% paraformaldehyde (in PBS) for 30 min. Then, the samples were deposited onto a 400-mesh carbon-coated copper grid and incubated for 10 min at room temperature. Excess samples

were blotted with filter paper and rinsed 5 times with water. Grids were dried for TEM imaging by a Tecnai 12 Quick Cryo-EM (FEI). For immunogold staining, the prepared DTC tEV samples were incubated with monoclonal mouse IgG human CD63 antibody (1:100 v/v, R&D systems) for 30 min, followed by incubation with antimouse nanogold (12 nm, 1:50 dilution) for 1 h. These gold-labeled samples were deposited onto carbon coated copper grids and incubated for 10 min. After rinsing 5 times using water, the grids were then dried for TEM imaging.

SEM Characterization of DTC tEVs

To characterize the distribution of DTC tEV on Click Beads after enrichment, Click Beads were incubated with 4% paraformaldehyde for 30 min at room temperature. Next, Click Beads were washed with water, deposited on a silicon wafer, and air-dried. The substrates were sputter-coated with gold and imaged under a ZEISS Supra 40VP SEM.

NTA Characterization of DTC tEVs

The size distribution and concentration of DTC tEVs were determined using nanoparticle tracking analysis (NTA) by ZetaView PMX-120 (Particle-Metrix, Germany). Samples were diluted into 0.22 μm filtered PBS at appropriate dilution rate ranging from 100 to 10,000-fold dilution. Each sample was replicated in three runs.

Statistical Analysis

Differences between two groups were determined using a two-sample t-test if data followed a normal distribution (ie, Fig. 5C-E, Fig. S2E, Fig. S8, Fig. S9, and Fig. S10) or nonparametric Mann-Whitney U test if data doesn't follow a normal distribution (ie, Fig. 3C-F, Fig. 6B, Fig. S4A-B, Fig. S5, Fig. S6 and Fig S7B-G). Differences among multiple groups were determined using one-way ANOVA if data followed a normal distribution and homogeneity of variance (ie, Fig. S2B-D). The logistic regression model, AUROC, and all the other statistical tests in this study were conducted using IBM SPSS statistics 23 and GraphPad prism 8.0 software. The optimal cut points were calculated to maximize sensitivity and specificity for ROC analysis. All tests were two-sided and $p < 0.05$ was considered significant, and $p < 0.01$ was considered highly significant.

Acknowledgements

We acknowledge all the patients and healthy donors who participated in this study. We thank Lucy Ruoxi Shi from Harvard-Westlake School for her design and creation of the cartoon illustration for this project. This work was supported by National Institutes of Health (R01 CA218356, R01 CA255727, R01 CA277530, R01 CA253651, U01 CA198900, and U01 EB026421).

Appendix A. Supporting information

Supplementary data associated with this article can be found in the online version

Received: ((will be filled in by the editorial staff))
Revised: ((will be filled in by the editorial staff))
Published online: ((will be filled in by the editorial staff))

Reference

[1] G. Siravegna, S. Marsoni, S. Siena, A. Bardelli, Nat Rev Clin Oncol, 14 (2017) 531-548.
[2] S.N. Lone, S. Nisar, T. Masoodi, M. Singh, A. Rizwan, S. Hashem, W. El-Rifai, D. Bedognetti, S.K. Batra, M. Haris, A.A. Bhat, M.A. Macha, Molecular cancer, 21 (2022) 79.
[3] K. Pantel, C. Alix-Panabieres, Nat Rev Clin Oncol, 16 (2019) 409-424.
[4] R.B. Corcoran, B.A. Chabner, New Engl J Med, 379 (2018) 1754-1765.
[5] G. Mauri, P.P. Vitiello, A. Sogari, G. Crisafulli, A. Sartore-Bianchi, S. Marsoni, S. Siena, A. Bardelli, Brit J Cancer, 127 (2022) 394-407.
[6] D. Crosby, S. Bhatia, K.M. Brindle, L.M. Coussens, C. Dive, M. Emberton, S. Esener, R.C. Fitzgerald, S.S. Gambhir, P. Kuhn, T.R. Rebbeck, S. Balasubramanian, Science (New York, N.Y.), 375 (2022) 1244-+.
[7] V. Plaks, C.D. Koopman, Z. Werb, Science (New York, N.Y.), 341 (2013) 1186-1188.
[8] Z. Deng, S. Wu, Y. Wang, D. Shi, EBioMedicine, 83 (2022) 104237.
[9] A. Moller, R.J. Lobb, Nat Rev Cancer, 20 (2020) 697-709.
[10] R. Xu, A. Rai, M. Chen, W. Suwakulsiri, D.W. Greening, R.J. Simpson, Nat Rev Clin Oncol, 15 (2018) 617-638.
[11] Q. Wu, S.Y. Fu, H.Y. Xiao, J.X. Du, F. Cheng, S.S. Wan, H.J. Zhu, D. Li, F. Peng, X.G. Ding, L.H. Wang, Adv Sci, 10 (2023) e2204814.
[12] Z.W. Han, F.N. Wan, J.Q. Deng, J.X. Zhao, Y.K. Li, Y.J. Yang, Q. Jiang, B.Q. Ding, C. Liu, B. Dai, J.S. Sun, Nano Today, 38 (2021) 101203.
[13] L. Valihrach, P. Androvic, M. Kubista, Molecular aspects of medicine, 72 (2020) 100825.
[14] S. Anfossi, A. Babayan, K. Pantel, G.A. Calin, Nat Rev Clin Oncol, 15 (2018) 541-563.
[15] K. Jerabkova-Roda, A. Dupas, N. Osmani, V. Hyenne, J.G. Goetz, Trends Cancer, 8 (2022) 799-805.

[16] K. Pantel, M.R. Speicher, Oncogene, 35 (2016) 1216-1224.
[17] G. van Niel, G. D'Angelo, G. Raposo, Nat Rev Mol Cell Biol, 19 (2018) 213-228.
[18] F. Tian, C. Liu, L. Lin, Q. Chen, J. Sun, TrAC Trends in Analytical Chemistry, 117 (2019) 128-145.
[19] C. Keup, P. Mach, B. Aktas, M. Tewes, H.C. Kolberg, S. Hauch, M. Sprenger-Haussels, R. Kimmig, S. Kasimir-Bauer, Clin Chem, 64 (2018) 1054-1062.
[20] C. Keup, V. Suryaprakash, S. Hauch, M. Storbeck, P. Hahn, M. Sprenger-Haussels, H.C. Kolberg, M. Tewes, O. Hoffmann, R. Kimmig, S. Kasimir-Bauer, Genome Med, 13 (2021) 85.
[21] J.Q. Deng, C. Liu, J.S. Sun, Advanced Materials, (2023) e2303092.
[22] M.N. Zhao, D.D. Mi, B.E. Ferdows, Y.K. Li, R.J. Wang, J.J. Li, D. Patel, N. Kong, S.J. Shi, W. Tao, Nano Today, 42 (2022) 101361.
[23] K. Chen, P. Dopico, J. Varillas, J. Zhang, T.J. George, Z.H. Fan, Angew Chem Int Ed Engl, 58 (2019) 7606-7610.
[24] J. Wu, X. Wei, J. Gan, L. Huang, T. Shen, J. Lou, B. Liu, J.X. Zhang, K. Qian, Advanced functional materials, 26 (2016) 4016-4025.
[25] Y.T. Kang, T. Hadlock, T.W. Lo, E. Purcell, A. Mutukuri, S. Fouladdel, M.D. Raguera, H. Fairbairn, V. Murlidhar, A. Durham, S.A. McLean, S. Nagrath, Adv Sci, 7 (2020) 2001581.
[26] X.F. Chen, H.M. Ding, D.D. Zhang, K.F. Zhao, J.F. Gao, B.Q. Lin, C. Huang, Y.L. Song, G. Zhao, Y.Q. Ma, L.L. Wu, C.Y. Yang, Adv Sci, 8 (2021) e2102070.
[27] N. Sun, C. Zhang, J. Wang, X. Yue, H.Y. Kim, R.Y. Zhang, H. Liu, J. Widjaja, H. Tang, T.X. Zhang, J. Ye, A. Qian, C. Liu, A. Wu, K. Wang, M. Johanis, P. Yang, H. Liu, M. Meng, L. Liang, R. Pei, W. Chai-Ho, Y. Zhu, H.R. Tseng, Nano today, 49 (2023) 101786.
[28] G.Y. Qiu, A. Thakur, C. Xu, S.P. Ng, Y. Lee, C.M.L. Wu, Adv Funct Mater, 29 (2019) 1806761.
[29] P. Sharma, S. Ludwig, L. Muller, C.S. Hong, J.M. Kirkwood, S. Ferrone, T.L. Whiteside, J Extracell Vesicles, 7 (2018) 1435138.
[30] J.J. Wang, N. Sun, Y.T. Lee, M. Kim, T. Vagner, K. Rohena-Rivera, Z. Wang, Z. Chen, R.Y. Zhang, J. Lee, C. Zhang, H. Tang, J. Widjaja, T.X. Zhang, D. Qi, P.C. Teng, Y.J. Jan, K.C. Hou, C. Hamann, H.M. Sandler, T.J. Daskivich, D.J. Luthringer, N.A. Bhowmick, R. Pei, S. You, D. Di Vizio, H.R. Tseng, J.F. Chen, Y. Zhu, E.M. Posadas, Nano Today, 48 (2023) 101746.
[31] J. Dong, Y.J. Jan, J. Cheng, R.Y. Zhang, M. Meng, M. Smalley, P.J. Chen, X. Tang, P. Tseng, L. Bao, T.Y. Huang, D. Zhou, Y. Liu, X. Chai, H. Zhang, A. Zhou, V.G. Agopian, E.M. Posadas, J.J. Shyue, S.J. Jonas, P.S. Weiss, M. Li, G. Zheng, H.H. Yu, M. Zhao, H.R. Tseng, Y. Zhu, Sci Adv, 5 (2019) eaav9186.
[32] N. Sun, C. Zhang, Y.T. Lee, B.V. Tran, J. Wang, H. Kim, J. Lee, R.Y. Zhang, J.J. Wang, J. Hu, Z. Zhang, M.S. Alsudaney, K.C. Hou, H. Tang, T.X. Zhang, I.Y. Liang, Z. Zhou, M. Chen, A.H. Yeh, W. Li, X.J. Zhou, H.R. Chang, S.B. Han, S. Sadeghi, R.S. Finn, S. Saab, R.W. Busuttil, M. Noureddin, W.S. Ayoub, A. Kuo, V. Sundaram, B. Al-Ghaieb, J. Palomique, K. Kosari, I.K. Kim, T. Todo, N.N. Nissen, M.L. Tomasi, S. You, E.M. Posadas, J.X. Wu, M. Wadehra, M.S. Sim, Y. Li, H.L. Wang, S.W. French, S.C. Lu, L. Wu, R. Pei, L. Liang, J.D. Yang, V.G. Agopian, H.R. Tseng, Y. Zhu, Hepatology, 77 (2023) 774-788.
[33] M.L. Blackman, M. Royzen, J.M. Fox, J Am Chem Soc, 130 (2008) 13518-13519.
[34] M.R. Karver, R. Weissleder, S.A. Hilderbrand, Bioconjug Chem, 22 (2011) 2263-2270.
[35] D. Bauer, M.A. Cornejo, T.T. Hoang, J.S. Lewis, B.M. Zeglis, Bioconjug Chem, (2023) 1925-1950.
[36] W.X. Xi, T.F. Scott, C.J. Kloxin, C.N. Bowman, Adv Funct Mater, 24 (2014) 2572-2590.

[37] J.W. Franses, J. Philipp, P. Missios, I. Bhan, A. Liu, C. Yashaswini, E. Tai, H. Zhu, M. Ligorio, B. Nicholson, E.M. Tassoni, N. Desai, A.S. Kulkarni, A. Szabolcs, T.S. Hong, A.S. Liss, C. Fernandez-Del Castillo, D.P. Ryan, S. Maheswaran, D.A. Haber, G.Q. Daley, D.T. Ting, Nature communications, 11 (2020) 3303.
[38] N.H. Stoecklein, G. Fluegen, R. Guglielmi, R.P.L. Neves, T. Hackert, E. Birgin, S.A. Cieslik, M. Sudarsanam, C. Driemel, G. van Dalum, A. Franken, D. Niederacher, H. Neubauer, T. Fehm, J.M. Rox, P. Böhme, L. Häberle, W. Göring, I. Esposito, S.A. Topp, F.A.W. Coumans, J. Weitz, W.T. Knoefel, J.C. Fischer, U. Bork, N.N. Rahbari, Molecular cancer, 22 (2023) 181.
[39] A. Miranda, J. Lortet-Tieulent, F. Bray, B.C. Cao, S. Franceschi, S. Vaccarella, L. Dal Maso, Lancet Diabetes Endo, 9 (2021) 225-234.
[40] M. Pizzato, M.M. Li, J. Vignat, M. Laversanne, D. Singh, C. La Vecchia, S. Vaccarella, Lancet Diabetes Endo, 10 (2022) 264-272.
[41] D.W. Chen, B.H.H. Lang, D.S.A. McLeod, K. Newbold, M.R. Haymart, Lancet (London, England), 401 (2023) 1531-1544.
[42] W.W. Wang, Z.Y. Zheng, J.Y. Lei, Int J Mol Sci, 24 (2023) 13767.
[43] M. Luster, T. Weber, F.A. Verburg, Nat Rev Endocrinol, 10 (2014) 563-574.
[44] F. Khatami, B. Larijani, S. Nasiri, S.M. Tavangar, Int J Mol Cell Med, 8 (2019) 19-29.
[45] N. Sun, B.V. Tran, Z. Peng, J. Wang, C. Zhang, P. Yang, T.X. Zhang, J. Widjaja, R.Y. Zhang, W. Xia, A. Keir, J.W. She, H.H. Yu, J.J. Shyue, H. Zhu, V.G. Agopian, R. Pei, J.S. Tomlinson, J.A. Toretsky, S.J. Jonas, N. Federman, S. Lu, H.R. Tseng, Y. Zhu, Adv Sci (Weinh), 9 (2022) e2105853.
[46] N. Sun, Y.T. Lee, M. Kim, J.J. Wang, C. Zhang, P.C. Teng, D. Qi, R.Y. Zhang, B.V. Tran, Y.T. Lee, J. Ye, J. Palomique, N.N. Nissen, S.B. Han, S. Sadeghi, R.S. Finn, S. Saab, R.W. Busuttil, E.M. Posadas, L. Liang, R. Pei, J.D. Yang, S. You, V.G. Agopian, H.R. Tseng, Y. Zhu, Adv Mater Technol, 6 (2021) 2001056.
[47] F.A. Coumans, S.T. Ligthart, J.W. Uhr, L.W. Terstappen, Clinical cancer research : an official journal of the American Association for Cancer Research, 18 (2012) 5711-5718.
[48] J.M. Hou, M.G. Krebs, L. Lancashire, R. Sloane, A. Backen, R.K. Swain, L.J. Priest, A. Greystoke, C. Zhou, K. Morris, T. Ward, F.H. Blackhall, C. Dive, J Clin Oncol, 30 (2012) 525-532.
[49] L. Wang, Y. Li, J. Xu, A. Zhang, X. Wang, R. Tang, X. Zhang, H. Yin, M. Liu, D.D. Wang, P.P. Lin, L. Shen, J. Dong, Cancer Lett, 412 (2018) 99-107.
[50] H.J. Yoon, T.H. Kim, Z. Zhang, E. Azizi, T.M. Pham, C. Paoletti, J. Lin, N. Ramnath, M.S. Wicha, D.F. Hayes, D.M. Simeone, S. Nagrath, Nat Nanotechnol, 8 (2013) 735-741.
[51] T.H. Kim, Y. Wang, C.R. Oliver, D.H. Thamm, L. Cooling, C. Paoletti, K.J. Smith, S. Nagrath, D.F. Hayes, Nature communications, 10 (2019) 1478.
[52] S. Liu, Z. Tian, L. Zhang, S. Hou, S. Hu, J. Wu, Y. Jing, H. Sun, F. Yu, L. Zhao, R. Wang, H.R. Tseng, H.E. Zhau, L.W. Chung, K. Wu, H. Wang, J.B. Wu, Y. Nie, C. Shao, Oncotarget, 7 (2016) 59877-59891.
[53] W. He, M. Hou, H. Zhang, C. Zeng, S. He, X. Chen, M. Xu, C. Sun, W. Jiang, H. Wang, H. Shen, Y. Zhang, J. Liu, S. Sun, N. Jiang, Y. Cui, Y. Sun, Y. Chen, J. Cao, C. Wang, M. Li, Y. Zhang, L. Wang, J. Wang, M. Lin, Z. Ke, International journal of cancer, 144 (2019) 1421-1431.
[54] C. Ensinger, R. Kremser, R. Prommegger, G. Spizzo, K.W. Schmid, J Immunother, 29 (2006) 569-573.
[55] H. Tan, K. Ye, Z.M. Wang, H.H. Tang, Transl Res, 152 (2008) 143-149.

[56] J. Kowal, G. Arras, M. Colombo, M. Jouve, J.P. Morath, B. Primdal-Bengtson, F. Dingli, D. Loew, M. Tkach, C. Thery, Proceedings of the National Academy of Sciences of the United States of America, 113 (2016) E968-977.
[57] D. Lin, L. Shen, M. Luo, K. Zhang, J. Li, Q. Yang, F. Zhu, D. Zhou, S. Zheng, Y. Chen, J. Zhou, Signal transduction and targeted therapy, 6 (2021) 404.
[58] G. Bordanaba-Florit, F. Royo, S.G. Kruglik, J.M. Falcon-Perez, Nat Protoc, 16 (2021) 3163-3185.
[59] E. Willms, C. Cabanas, I. Mager, M.J.A. Wood, P. Vader, Front Immunol, 9 (2018) 738.
[60] S. Ferguson, K.S. Yang, P. Zelga, A.S. Liss, J.C.T. Carlson, C.F. Del Castillo, R. Weissleder, Sci Adv, 8 (2022) eabm3453.
[61] I.J. Purvis, K.K. Velpula, M.R. Guda, D. Nguyen, A.J. Tsung, S. Asuthkar, Int J Mol Sci, 21 (2020) 7050.
[62] X.X. Zhan, B. Zhao, C. Diao, Y. Cao, R.C. Cheng, Endocrine pathology, 26 (2015) 21-26.
[63] B. Zhao, Z. Huang, X. Zhu, H. Cai, Y. Huang, X. Zhang, Z. Zhang, H. Lu, C. An, L. Niu, Z. Li, Front Cell Dev Biol, 10 (2022) 819236.
[64] E.C. Morari, J.R. Silva, A.C. Guilhen, L.L. Cunha, M.A. Marcello, F.A. Soares, J. Vassallo, L.S. Ward, Endocrine pathology, 21 (2010) 242-249.
[65] K.Q. Peng, Y.J. Yan, S.P. Gao, J. Zhu, Adv Mater, 14 (2002) 1164-1167.
[66] Y. Afshar, J. Dong, P. Zhao, L. Li, S. Wang, R.Y. Zhang, C. Zhang, O. Yin, C.S. Han, B.D. Einerson, T.L. Gonzalez, H. Zhang, A. Zhou, Z. Yang, S.J. Chou, N. Sun, J. Cheng, H. Zhu, J. Wang, T.X. Zhang, Y.T. Lee, J.J. Wang, P.C. Teng, P. Yang, D. Qi, M. Zhao, M.S. Sim, R. Zhe, J.D. Goldstein, J. Williams, 3rd, X. Wang, Q. Zhang, L.D. Platt, C. Zou, M.D. Pisarska, H.R. Tseng, Y. Zhu, Nature communications, 12 (2021) 4408.
[67] W. Gao, T. Huang, H. Yuan, J. Yang, Q. Jin, C. Jia, G. Mao, J. Zhao, Talanta, 185 (2018) 229-236.
[68] X. Lu, S. Tan, M. Wu, H. Ju, X. Liang, P. Li, Colloids and surfaces. B, Biointerfaces, 199 (2021) 111542.
[69] W. Xu, L. Cao, L. Chen, J. Li, X.F. Zhang, H.H. Qian, X.Y. Kang, Y. Zhang, J. Liao, L.H. Shi, Y.F. Yang, M.C. Wu, Z.F. Yin, Clin Cancer Res, 17 (2011) 3783-3793.
[70] M. Uhlen, L. Fagerberg, B.M. Hallstrom, C. Lindskog, P. Oksvold, A. Mardinoglu, A. Sivertsson, C. Kampf, E. Sjostedt, A. Asplund, I. Olsson, K. Edlund, E. Lundberg, S. Navani, C.A. Szigyarto, J. Odeberg, D. Djureinovic, J.O. Takanen, S. Hober, T. Alm, P.H. Edqvist, H. Berling, H. Tegel, J. Mulder, J. Rockberg, P. Nilsson, J.M. Schwenk, M. Hamsten, K. von Feilitzen, M. Forsberg, L. Persson, F. Johansson, M. Zwahlen, G. von Heijne, J. Nielsen, F. Ponten, Science (New York, N.Y.), 347 (2015) 1260419.
[71] N.Y.L. Yu, B.M. Hallstrom, L. Fagerberg, F. Ponten, H. Kawaji, P. Carninci, A.R.R. Forrest, Y. Hayashizaki, M. Uhlen, C.O. Daub, F. Consortium, Nucleic Acids Res, 43 (2015) 6787-6798.
[72] J.A. Welsh, D.C.I. Goberdhan, L. O'Driscoll, E.I. Buzas, C. Blenkiron, B. Bussolati, H. Cai, D. Di Vizio, T.A.P. Driedonks, U. Erdbrugger, J.M. Falcon-Perez, Q.L. Fu, A.F. Hill, M. Lenassi, S.K. Lim, M.G. Mahoney, S. Mohanty, A. Moller, R. Nieuwland, T. Ochiya, S. Sahoo, A.C. Torrecilhas, L. Zheng, A. Zijlstra, S. Abuelreich, R. Bagabas, P. Bergese, E.M. Bridges, M. Brucale, D. Burger, R.P. Carney, E. Cocucci, R. Crescitelli, E. Hanser, A.L. Harris, N.J. Haughey, A. Hendrix, A.R. Ivanov, T. Jovanovic-Talisman, N.A. Kruh-Garcia, V. Ku'ulei-Lyn Faustino, D. Kyburz, C. Lasser, K.M. Lennon, J. Lotvall, A.L. Maddox, E.S. Martens-Uzunova, R.R. Mizenko, L.A. Newman, A. Ridolfi, E. Rohde, T. Rojalin, A. Rowland, A. Saftics, U.S. Sandau, J.A. Saugstad, F. Shekari, S. Swift, D. Ter-Ovanesyan, J.P. Tosar, Z. Useckaite, F. Valle, Z. Varga, E. van der Pol, M.J.C. van Herwijnen, M.H.M.

Wauben, A.M. Wehman, S. Williams, A. Zendrini, A.J. Zimmerman, M. Consortium, C. Thery, K.W. Witwer, J Extracell Vesicles, 13 (2024) e12404.
[73] S. Wang, K. Liu, J. Liu, Z.T. Yu, X. Xu, L. Zhao, T. Lee, E.K. Lee, J. Reiss, Y.K. Lee, L.W. Chung, J. Huang, M. Rettig, D. Seligson, K.N. Duraiswamy, C.K. Shen, H.R. Tseng, Angew Chem Int Ed Engl, 50 (2011) 3084-3088.
[74] J. Dong, R.Y. Zhang, N. Sun, J. Hu, M.D. Smalley, A. Zhou, H. Yue, W. Rothermich, M. Chen, J. Chen, J. Ye, P.C. Teng, D. Qi, J.A. Toretsky, J.S. Tomlinson, M. Li, P.S. Weiss, S.J. Jonas, N. Federman, L. Wu, M. Zhao, H.R. Tseng, Y. Zhu, Advanced functional materials, 30 (2020) 2003237.
[75] Y.J. Jan, J. Yoon, J.F. Chen, P.C. Teng, N. Yao, S. Cheng, A. Lozano, G.C.Y. Chu, H. Chung, Y.T. Lu, P.J. Chen, J.J. Wang, Y.T. Lee, M. Kim, Y. Zhu, B.S. Knudsen, F.Y. Feng, I.P. Garraway, A.C. Gao, L.W.K. Chung, M.R. Freeman, S. You, H.R. Tseng, E.M. Posadas, Theranostics, 9 (2019) 2812-2826.

Table 1. Clinical characteristics of DTC patients

Characteristic		DTC, n = 38
Median Age		46.5(24-78)
Male		14
Female		24
BMI		26.18±4.40
Median tumor diameter (cm)		1.5(0.1-8.8)
Number of lesions		
	Single	21
	Multiple	17
The T stages		
	T1	22
	T2	6
	T3	9
	T4	1
Lymph node involvement		
	N0	20
	N1	18
Presence of metastasis		
	M0	38
	M1	0